

Gravity On-shell Diagrams

Enrico Herrmann,¹ Jaroslav Trnka²

¹ *Walter Burke Institute for Theoretical Physics,
California Institute of Technology, Pasadena, CA 91125, USA*

² *Center for Quantum Mathematics and Physics (QMAP),
Department of Physics, University of California, Davis, CA 95616, USA*

E-mail: eherrmann@caltech.edu, trnka@ucdavis.edu

ABSTRACT: We study on-shell diagrams for gravity theories with any number of supersymmetries and find a compact Grassmannian formula in terms of edge variables of the graphs. Unlike in gauge theory where the analogous form involves only $d \log$ -factors, in gravity there is a non-trivial numerator as well as higher degree poles in the edge variables. Based on the structure of the Grassmannian formula for $\mathcal{N} = 8$ supergravity we conjecture that gravity loop amplitudes also possess similar properties. In particular, we find that there are only logarithmic singularities on cuts with finite loop momentum, poles at infinity are present and loop amplitudes show special behavior on certain collinear cuts. We demonstrate on 1-loop and 2-loop examples that the behavior on collinear cuts is a highly non-trivial property which requires cancellations between all terms contributing to the amplitude.

Contents

1	Introduction	1
1.1	On-shell diagrams	2
1.2	Grassmannian formulation	7
1.3	Hidden properties of $\mathcal{N} = 4$ sYM amplitudes	12
2	Non-planar on-shell diagrams	13
2.1	First look: MHV leading singularities	14
2.2	Three point amplitudes with spin s	17
2.3	Grassmannian formula	19
3	Properties of gravity on-shell diagrams	21
3.1	Calculating on-shell diagrams	21
3.2	More examples	24
3.3	Structure of singularities	26
4	From on-shell diagrams to scattering amplitudes	29
4.1	Non-planar $\mathcal{N} = 4$ sYM amplitudes	30
4.2	Gravity from Yang-Mills	32
4.3	Collinear behavior	34
5	Conclusion	40

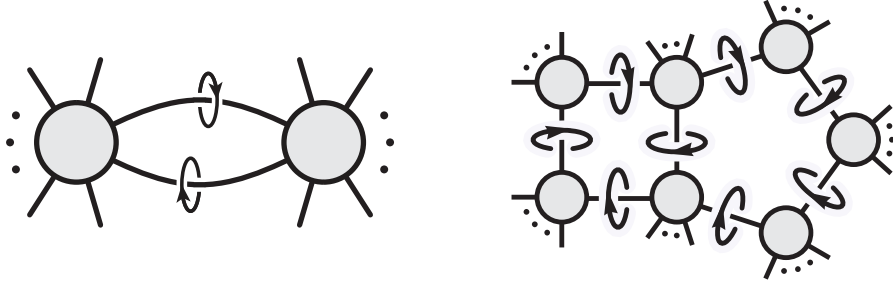
1 Introduction

Within the field of scattering amplitudes, a great number of developments in the last decade or so are based on powerful on-shell methods [1–7]. Amongst others, BCFW-recursion [1, 2] and generalized unitarity [3–5] allowed to push the boundary of computable amplitudes in terms of number of loops and legs. The core idea behind these methods is that on-shell amplitudes break up into products of simpler amplitudes on all factorization channels. In the traditional picture of Quantum Field Theory, locality and unitarity dictate the form and locations of all these residues. In particular, they arise in kinematic regions where either internal particles or sums of external particles become on-shell. Associated with these residues are vanishing propagators and in this

context we talk about *cuts* of the amplitude. Symbolically, one can write the two types of elementary cuts (singularities) as [8],

$$\partial \left| \text{Amplitude with } \mathcal{A}_n^\ell \right| = \sum_{L,R} \text{Diagram with } L \text{ and } R \text{ connected by a red line} + \sum_a \text{Diagram with } \mathcal{A}_{n+2}^{\ell-1} \text{ and a blue loop} \quad (1.1)$$

where the first term corresponds to the factorization into a product of lower point amplitudes (keeping the total loop degree fixed) while the second term is the forward limit of an $(L - 1)$ -loop, $(n + 2)$ -point amplitude. In general field theories this term suffers from IR-divergencies [9] and therefore, in many cases the fundamental cut is the well-known *unitarity cut* [10, 11]. Iterating these cuts one can calculate multi-dimensional residues by setting an increasing number of propagators to zero. This is known in the literature as *generalized unitarity* [3–5].



Generically, it is not possible to set to zero more than two propagators in a given loop while simultaneously also requiring real kinematics. Therefore, the loop momenta are complex when constrained by the set of on-shell conditions which implies that these singularities are outside the physical integration region. The main success of generalized unitarity then relies on the fact that the integrands are rational functions that can be analytically continued so that complex residues (given by a sufficient set of cuts) completely specify them.

A natural next step in this line of thought is to cut the maximum number of propagators which factorizes the amplitude into the simplest building blocks [5]. The most elementary case occurs when all factors are three-point amplitudes. As we will describe in a moment, these are rather special due to the particular features of three-point kinematics. In this scenario we talk about *on-shell diagrams* [12].

1.1 On-shell diagrams

For massless particles, the three-point amplitudes are completely fixed by Poincare symmetry to all loop orders in perturbation theory up to an overall constant [13]. This

statement holds in any Quantum Field Theory with massless states and just follows from the fact that there are no kinematic invariants one can build out of three on-shell momenta. For real external kinematics, the on-shell conditions, $p_1^2 = p_2^2 = p_3^2 = 0$ and momentum conservation $p_1 + p_2 + p_3 = 0$ would force all three point amplitudes to vanish. However, for complex kinematics in $D = 4$ we have two distinct solutions [14] which can be conveniently written using spinor-helicity [15] variables $p^\mu = \sigma_{a\dot{a}}^\mu \lambda_a \tilde{\lambda}_{\dot{a}}$.

$$\text{I.) } \tilde{\lambda}_1 \sim \tilde{\lambda}_2 \sim \tilde{\lambda}_3 \text{ (MHV)}, \quad \text{II.) } \lambda_1 \sim \lambda_2 \sim \lambda_3 \text{ (}\overline{\text{MHV}}\text{)}.$$

Any three-point amplitude is then either of type I.) or II.). In particular, for the gluon-amplitudes in Yang-Mills theory we have two elementary amplitudes with MHV (+ − −) or $\overline{\text{MHV}}$ (− + +) helicity configuration (ignoring higher dimensional operators that could lead to (± ± ±) amplitudes, see e.g. [16]). In the maximally supersymmetric case of $\mathcal{N} = 4$ sYM theory these gluonic amplitudes are embedded in the MHV, resp. $\overline{\text{MHV}}$ superamplitudes (see e.g. [17]) which we denote by blobs with different colors,

$$\begin{array}{c} 2 \\ \diagup \\ 1 \text{ --- } \text{blue blob} \diagdown \\ 3 \end{array} = \frac{\delta^4(P) \delta^8(\mathcal{Q})}{\langle 12 \rangle \langle 23 \rangle \langle 31 \rangle}, \quad \begin{array}{c} 2 \\ \diagup \\ 1 \text{ --- } \text{white blob} \diagdown \\ 3 \end{array} = \frac{\delta^4(P) \delta^4(\tilde{\mathcal{Q}})}{[12][23][31]}, \quad (1.2)$$

where $\langle ij \rangle = \epsilon_{\alpha\beta} \lambda_i^\alpha \lambda_j^\beta$ and $[ij] = \epsilon_{\dot{\alpha}\dot{\beta}} \tilde{\lambda}_i^{\dot{\alpha}} \tilde{\lambda}_j^{\dot{\beta}}$. Using the anti-commuting $\tilde{\eta}^I$, $I = 1, \dots, 4$ variables to write the on-shell multiplet as [18],

$$\Phi(\tilde{\eta}) = g^+ + \tilde{\eta}^I \tilde{g}_I + \frac{1}{2!} \tilde{\eta}^I \tilde{\eta}^J \phi_{IJ} + \frac{1}{3!} \epsilon_{IJKL} \tilde{\eta}^I \tilde{\eta}^J \tilde{\eta}^K \tilde{g}^L + \frac{1}{4!} \epsilon_{IJKL} \tilde{\eta}^I \tilde{\eta}^J \tilde{\eta}^K \tilde{\eta}^L g^-$$

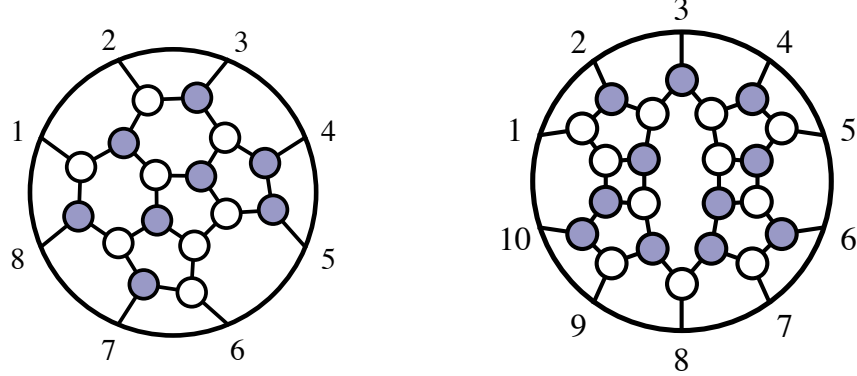
the arguments of the respective delta-functions in (1.2) are given by (neglecting all spinor- and $SU(4)$ R -symmetry indices),

$$P \equiv \lambda \cdot \tilde{\lambda} = \lambda_1 \tilde{\lambda}_1 + \lambda_2 \tilde{\lambda}_2 + \lambda_3 \tilde{\lambda}_3, \quad \mathcal{Q} \equiv \lambda \cdot \tilde{\eta} = \lambda_1 \tilde{\eta}_1 + \lambda_2 \tilde{\eta}_2 + \lambda_3 \tilde{\eta}_3, \quad \tilde{\mathcal{Q}} = [12] \tilde{\eta}_3 + [23] \tilde{\eta}_1 + [31] \tilde{\eta}_2.$$

Here and in the following we denote $\lambda \cdot \tilde{\lambda} \equiv \sum_{a=1}^n \lambda_a \tilde{\lambda}_a$, $\lambda \cdot \tilde{\eta} \equiv \sum_{a=1}^n \lambda_a \tilde{\eta}_a$ as the sum over all external particles.

Having completed the discussion of three-particle amplitudes, we are now in the position to introduce on-shell diagrams. For us, an on-shell diagram is any graph

formed from the two types of three-point amplitudes (1.2) connected by edges,

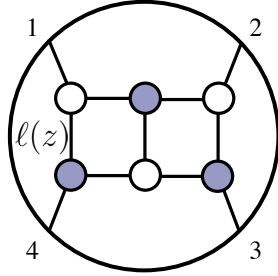


that all represent on-shell particles (both internal and external). In this section we review properties of on-shell diagrams in planar $\mathcal{N} = 4$ sYM and introduce all concepts relevant for our gravity discussion later. Further details can be found directly in [12] and the review article [19]. With this definition, the value of the diagram is given by the product of three-point amplitudes satisfying the on-shell conditions for all edges. In practice, the delta functions of the elementary three-point amplitudes can be used for solving for λ_I , $\tilde{\lambda}_I$ and $\tilde{\eta}_I$ of the internal particle and writing the overall result (including delta functions), using external data only. In this case we talk about *leading singularities* [7]. If the number of on-shell conditions exceeds the number of internal degrees of freedom, we get additional constraints on the external kinematics, while in the opposite case the on-shell diagram depends on some unfixed parameters. These cases are easily classified by a parameter n_δ counting the number of constraints on external kinematics $n_\delta = 0$, $n_\delta > 0$ and $n_\delta < 0$.

The simplest example of a reduced on-shell diagram ($n_\delta = 0$) actually represents the color-ordered four-point tree-level amplitude which consists of four vertices. The simpler looking on-shell diagram with only two vertices is the residue of the amplitude on the t -channel factorization pole and imposes a constraint ($n_\delta = 1$) on the external momenta.

$$\begin{aligned}
 \text{Diagram 1} &= \frac{\delta^4(\lambda \cdot \tilde{\lambda}) \delta^8(\lambda \cdot \tilde{\eta})}{\langle 12 \rangle \langle 23 \rangle \langle 34 \rangle \langle 41 \rangle} \\
 \text{Diagram 2} &= \frac{\delta^4(\lambda \cdot \tilde{\lambda}) \delta^8(\lambda \cdot \tilde{\eta}) \delta(\langle 14 \rangle)}{\langle 12 \rangle \langle 23 \rangle \langle 34 \rangle}
 \end{aligned}
 \tag{1.3}$$

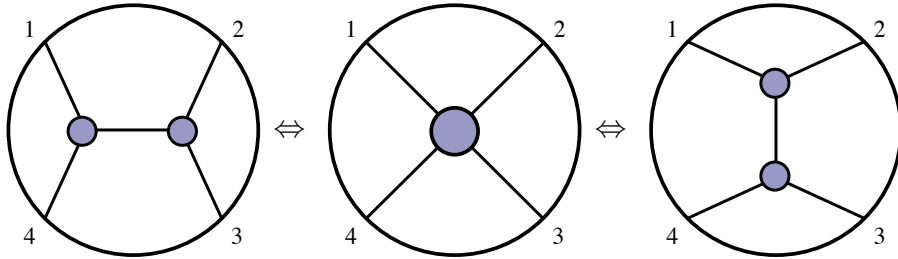
As an example for the third possibility ($n_\delta < 0$), we can draw a diagram which depends on one unfixed parameter z .



$$= \frac{\delta^4(\lambda \cdot \tilde{\lambda}) \delta^8(\lambda \cdot \tilde{\eta})}{z \langle 12 \rangle \langle 23 \rangle (\langle 34 \rangle + z \langle 31 \rangle) \langle 41 \rangle} \quad (1.4)$$

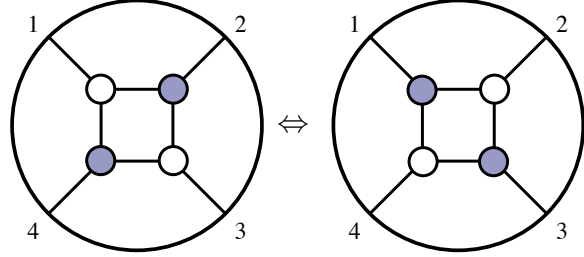
The counting is easy to understand if we think about the diagram as a hepta-cut of the two loop amplitude: there are seven on-shell conditions imposed on two off-shell loop momenta, leaving one degree of freedom unfixed. In the diagram z parametrizes the momentum flow along the edge between external legs 1 and 4, $\ell(z) = z \lambda_1 \tilde{\lambda}_4$ but also other internal legs will depend on z . In the standard approach of generalized unitarity, this diagram represents a *maximal cut* as there are no further propagators available to cut and localize the remaining degree of freedom. However, the amplitude does have further residues at $z = 0$ and $z = \frac{\langle 34 \rangle}{\langle 13 \rangle}$. Each residue corresponds to erasing an edge of (1.4) giving the one-loop on-shell diagram on the left of (1.3). This is a leading singularity of the amplitude – all degrees of freedom in loop momenta are fixed by on-shell conditions.

It turns out that not all on-shell diagrams are independent, but rather there are equivalence classes of diagrams related by certain identity moves. The first is the *merge and expand* move represented in (1.5). The black vertices enforce all $\tilde{\lambda}$'s to be proportional which is independent of the way the individual three-point amplitudes are connected,



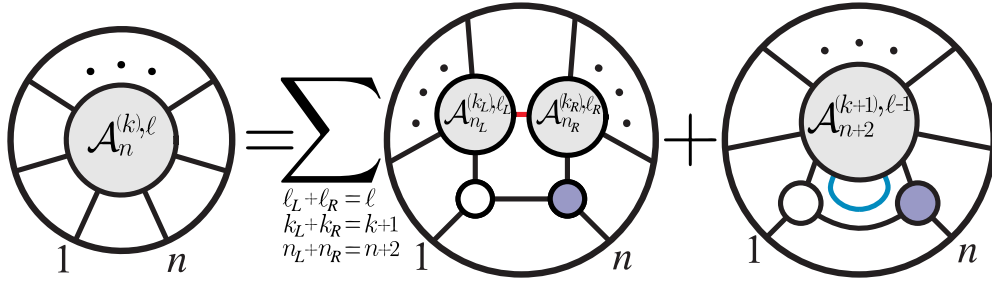
$$(1.5)$$

One further nontrivial move is the *square move* [20] which can be motivated by the cyclic invariance of the four-particle tree level amplitude,


(1.6)

Together with *bubble deletion* which does not play a role in our discussion here, these are all the equivalence moves for planar $\mathcal{N} = 4$ sYM. Modulo the aforementioned moves, it is possible to give a complete classification of on-shell diagrams [12] in this theory.

Besides representing cuts of loop amplitudes, on-shell diagrams serve directly as building blocks for constructing amplitudes. In particular, the BCFW recursion relation for tree-level amplitudes and loop integrands in planar $\mathcal{N} = 4$ sYM theory is represented by [8, 12]



This equation is a solution to the question what on-shell function has singularities given by (1.1). Here planarity was crucial because it permitted a unique definition of the *integrand* as a rational function with certain properties. It is this integrand which can be constructed recursively. The key point was the existence of global variables (dual variables and momentum twistors [21]) common to all terms in the expansion. Currently, it is the lack of global labels that hampers the extension of the recursion relations beyond the planar limit.

While the recursion relations are only formulated in planar $\mathcal{N} = 4$ sYM so far, the on-shell diagrams are well defined gauge invariant objects in any Quantum Field Theory, planar or non-planar, with or without supersymmetry. They are defined as products of on-shell three-point amplitudes (for theories with fundamental three point amplitudes) and at the least represent cuts of loop amplitudes. From that point of

view they encode an important amount of information about amplitudes in any theory and their properties are well worth studying in its own right.

1.2 Grassmannian formulation

Besides viewing on-shell diagrams as gluing of three-point amplitudes integrated over the on-shell phase space (including the sum over all physical states that can cross the cut) there is a completely different way how to calculate on-shell diagrams. This *dual formulation* expresses on-shell diagrams as differential forms on the (positive) Grassmannian [12]. There are a number of ways how to motivate this picture starting from classifying configurations of points with linear dependencies to representing the permutation group in terms of planar bi-colored graphs [22]. Physically, the most direct way to discover the Grassmannian picture for on-shell diagrams is to think about momentum conservation more seriously. Starting from the innocuous equation,

$$\delta^4(P) \equiv \delta^4(\lambda \cdot \tilde{\lambda}) = \delta^4(\lambda_1 \tilde{\lambda}_1 + \lambda_2 \tilde{\lambda}_2 + \cdots + \lambda_n \tilde{\lambda}_n), \quad (1.7)$$

one notes that this is a quadratic condition on the spinor-helicity variables. Naturally, one can ask if there is a way to trivialize the quadratic constraints and rewrite them as sets of linear relations between λ s and $\tilde{\lambda}$ s separately. The solution to this problem is to introduce an auxiliary k -plane in n -dimensions represented by a $(k \times n)$ -matrix C modulo a $GL(k)$ redundancy arising from row operations that leave the k -plane invariant. This space is known as the Grassmannian $G(k, n)$. Using these auxiliary variables, momentum conservation is then enforced geometrically [23–25] via the following set of delta functions (similar relations hold in twistor and momentum twistor spaces),

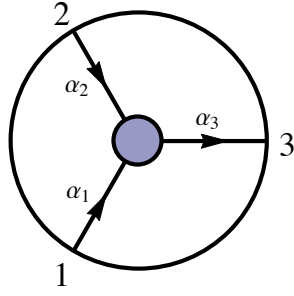
$$\delta^{(k \times 2)}(C_{\alpha a} \tilde{\lambda}_a) \delta^{((n-k) \times 2)}(C_{\beta a}^\perp \lambda_a), \quad (1.8)$$

where C^\perp denotes the $((n-k) \times n)$ -matrix orthogonal to C , $C \cdot C^\perp = 0$. There are $2n$ delta functions in total, four of them give the overall momentum conservation while the remaining $2n - 4$ constrain the parameters of the C -matrix.

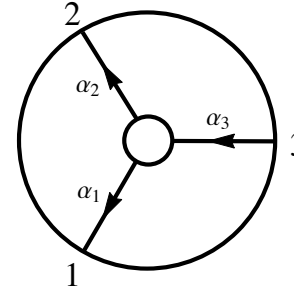
The study of Grassmannians is a vast and active topic in the mathematics community ranging, amongst others, from combinatorics to algebraic geometry [22, 26–30]. There is a close connection to on-shell diagrams which was simultaneously discovered both by physicists in the context of scattering amplitudes and by mathematicians (in the math literature these diagrams are called *plabic graphs*) in searching for positive parameterizations of Grassmannians. In particular, each on-shell diagram gives a parametrization for the C -matrix using a set of variables α_j . When these variables are real with definite signs, the matrix C has all main minors positive and then we talk about positive Grassmannian $G_+(k, n)$. These variables are associated with either

faces or edges of the diagram. The face variables are more invariant but they can be used only in planar diagrams. Since in this paper we will include non-planar examples we use *edge variables* instead to parametrize the Grassmannian matrix.

Like in the physical picture where on-shell diagrams are products of three-point amplitudes we also start our discussion with elementary three point vertices. We first choose a *perfect orientation* in which we attach arrows to all legs. For all black vertices two of the arrows are incoming and one outgoing while for white vertices one is incoming and two outgoing. Then we associate a (2×3) -matrix with the black (MHV, $k = 2$) vertex and a (1×3) -matrix with the white ($\overline{\text{MHV}}$, $k = 1$) vertex in the following way,



$$C = \begin{pmatrix} 1 & 0 & \alpha_1 \alpha_3 \\ 0 & 1 & \alpha_2 \alpha_3 \end{pmatrix}$$



$$C = (\alpha_1 \alpha_3 \quad \alpha_2 \alpha_3 \quad 1) .$$

(1.9)

Choosing a perfect orientation fixes a part of the general $GL(k)$ -redundancy of the C -matrix that represents a point in the Grassmannian. With the remaining $GL(1)_v$ -freedom we are allowed to fix any one of the variables associated to the half-edges of that vertex to some arbitrary value. The canonical choice would be $\alpha_3 = 1$, but any other finite, nonzero value is allowed as well. For the moment though, let us keep this freedom unfixed.

In the next step we glue the atomic three-point vertices together into an arbitrary planar on-shell diagram to which we associate some bigger $(k \times n)$ -matrix C . In the gluing process, we identify two half-edges of the vertices involved in the fusion to form an internal edge of the bigger on-shell diagram. Each internal edge of this big diagram is then parametrized by two variables $\alpha^{(1)}$ and $\alpha^{(2)}$ coming from the two vertices involved in the gluing process so that the C -matrix will only depend on their product $\alpha = \alpha^{(1)} \alpha^{(2)}$. Pictorially, this process is simple to state (the grey blob denotes

the rest of the diagram),

$$(1.10)$$

and illustrates that it is natural to directly use edge-variables α_k rather than the individual vertex variables introduced by the little Grassmannians. The identification is as follows; in the gluing process we encounter another $GL(1)_e$ redundancy stemming from the fact that the internal momentum of that edge is invariant under little group rescaling $\lambda_I \rightarrow t_I \lambda_I$, $\tilde{\lambda}_I \rightarrow t_I^{-1} \tilde{\lambda}_I$ which allows us to combine two of the vertex-variables into a single edge-variable. Doing this for all internal edges, we are only left with the $GL(1)_v$ redundancies for each vertex in the big on-shell diagram which we can use to set certain edge weights to one for instance.

$$(1.11)$$

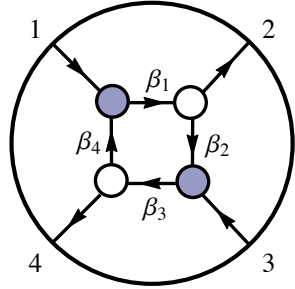
In terms of edge-variables, the rule how to obtain the C -matrix from the graph is quite simple. First, we have to choose a perfect orientation for the diagram by consistently decorating all edges with arrows. The external legs with incoming arrows are called *sources*, while the external legs with outgoing arrows are called *sinks*. For the diagram with k sources and $n - k$ sinks we construct a $(k \times n)$ matrix C . Note that these numbers do not depend on the way we choose a perfect orientation but are an invariant property of the on-shell diagram itself. Each row of the matrix is associated with one source while the columns are linked to both sources and sinks. Now each entry $C_{\alpha a}$ is calculated as

$$C_{\alpha a} = \sum_{\Gamma_{\alpha \rightarrow a}} \prod_j \alpha_j, \quad (1.12)$$

where we sum over all directed paths $\Gamma_{\alpha \rightarrow a}$ from the source α to the sink a by following the arrows. Along the way we take the product of all edge variables. If the label $a = \alpha$ is the same source we fix the matrix entry to 1 if $a = \alpha'$ is a different source the matrix entry is 0. For the examples above the C -matrices are,

$$C^{(a)} = \begin{pmatrix} 1 & \alpha_1 & 0 & \alpha_4 \\ 0 & \alpha_2 & 1 & \alpha_3 \end{pmatrix}, \quad C^{(b)} = \begin{pmatrix} 1 & \alpha_1 + \alpha_2 \alpha_6 & \alpha_6 & \alpha_3 \alpha_6 & 0 \\ 0 & \alpha_5 \alpha_6 \alpha_2 & \alpha_5 \alpha_6 & \alpha_4 + \alpha_3 \alpha_5 \alpha_6 & 1 \end{pmatrix}. \quad (1.13)$$

Different choices for the sources and sinks corresponds to different gauge fixings of the C -matrix that are related by $GL(k)$ -transformations. For some gauge choices, the perfect orientation can involve closed loops. In these cases there are infinitely many paths from α to a and we have to sum over all of them,



$$\Leftrightarrow C = \begin{pmatrix} 1 & \beta_1 \delta & 0 & \beta_1 \beta_2 \beta_3 \delta \\ 0 & \beta_3 \beta_4 \beta_1 \delta & 1 & \beta_3 \delta \end{pmatrix}, \quad (1.14)$$

where δ is given by a geometric series,

$$\delta = \sum_{\sigma=0}^{\infty} (\beta_1 \beta_2 \beta_3 \beta_4)^{\sigma} = \frac{1}{1 - \beta_1 \beta_2 \beta_3 \beta_4}. \quad (1.15)$$

The important connection between the Grassmannian formulation and physics is that the same on-shell diagram that labels the C -matrix also represents a cut of a scattering amplitude in planar $\mathcal{N} = 4$ sYM. The nontrivial relation is that the value of the on-shell diagram as calculated by multiplying three-point amplitudes is equal to the following differential form

$$d\Omega = \frac{d\alpha_1}{\alpha_1} \frac{d\alpha_2}{\alpha_2} \dots \frac{d\alpha_m}{\alpha_m} \delta(C \cdot Z). \quad (1.16)$$

All the dependence on external kinematics is pushed into the delta functions,

$$\delta(C \cdot Z) \equiv \delta^{(k \times 2)}(C_{ab} \tilde{\lambda}_b) \delta^{((n-k) \times 2)}(C_{cb}^{\perp} \lambda_b) \delta^{(k \times \mathcal{N})}(C_{ab} \tilde{\eta}_b) \quad (1.17)$$

which linearize both momentum and super-momentum conservation $\delta^4(P) \delta^8(\mathcal{Q})$ using the auxiliary Grassmannian C -matrix associated with the diagram. Depending on the details of the given diagram, the delta functions (1.17) allow us to fix a certain

number of edge variables α_j . In the case of on-shell diagrams relevant for tree-level amplitudes (leading singularities), all variables are fixed, while the on-shell diagrams appearing in the loop recursion relations have $4L$ unfixed parameters α_j which are related to the $4L$ degrees of freedom of L off-shell loop momenta ℓ_i .

So far, the $((n-k) \times n)$ -matrix C^\perp orthogonal to C , defined via $C \cdot C^\perp = 0$, has played no significant role in our discussion but is crucial for momentum conservation in (1.8) and (1.17). Given a gauge fixed C -matrix, there is a simple rule how to obtain C^\perp . One takes the $(n-k)$ columns of the C -matrix that correspond to the $(n-k)$ sinks of the on-shell diagram. For each such column of C , one forms a row of C^\perp by writing the negative entries of the column into the slots that correspond to the sources. The remaining $((n-k) \times (n-k))$ matrix entries of C^\perp are then filled by a $((n-k) \times (n-k))$ identity-matrix. Let us apply the construction procedure to some concrete examples. For the C -matrices in (1.13) corresponding to the on-shell diagrams (1.11), we get the following C^\perp -matrices,

$$C_{(a)}^\perp = \begin{pmatrix} -\alpha_1 & 1 & -\alpha_2 & 0 \\ -\alpha_4 & 0 & -\alpha_3 & 1 \end{pmatrix}, \quad C_{(b)}^\perp = \begin{pmatrix} -(\alpha_1 + \alpha_2\alpha_6) & 1 & 0 & 0 & -\alpha_5\alpha_6\alpha_2 \\ -\alpha_6 & 0 & 1 & 0 & -\alpha_5\alpha_6 \\ -\alpha_6\alpha_3 & 0 & 0 & 1 & -(\alpha_4 + \alpha_5\alpha_6\alpha_3) \end{pmatrix}. \quad (1.18)$$

Now that we have all ingredients together, we can go ahead and consider a simple on-shell diagram in detail. Specifically, we calculate the box on-shell diagram (1.11)(a), in which case the delta functions (1.17) are equal to

$$\delta(C \cdot Z) = \frac{1}{\langle 13 \rangle^4} \delta \left[\alpha_1 - \frac{\langle 23 \rangle}{\langle 13 \rangle} \right] \delta \left[\alpha_2 - \frac{\langle 12 \rangle}{\langle 13 \rangle} \right] \delta \left[\alpha_3 - \frac{\langle 14 \rangle}{\langle 13 \rangle} \right] \delta \left[\alpha_4 - \frac{\langle 43 \rangle}{\langle 13 \rangle} \right] \delta^4(P) \delta^8(\mathcal{Q}) \quad (1.19)$$

and the differential form becomes a function of external kinematics only,

$$d\Omega = \frac{d\alpha_1}{\alpha_1} \frac{d\alpha_2}{\alpha_2} \frac{d\alpha_3}{\alpha_3} \frac{d\alpha_4}{\alpha_4} \delta(C \cdot Z) = \frac{\delta^4(P) \delta^8(\mathcal{Q})}{\langle 12 \rangle \langle 23 \rangle \langle 34 \rangle \langle 41 \rangle}. \quad (1.20)$$

This is equal to formula (1.3) found by multiplying three-point amplitudes.

The same procedure can be applied to planar on-shell diagrams in $\mathcal{N} < 4$ sYM. The important difference is that the diagrams are necessarily oriented unlike in the maximally supersymmetric case where the perfect orientations only played an auxiliary role for constructing the C -matrix. This corresponds to the fact that in less supersymmetric theories we need two on-shell multiplets to capture the positive and negative helicity gluons (and their respective superpartners) and the arrows specify which multiplet we are talking about. For the external states, we can choose the orientation of the arrows of a given on-shell diagram depending on the helicity structure we want to consider,

but for internal legs we have to sum over all possible orientations. In addition, for perfect orientations with closed internal loops we have to add an extra factor, \mathcal{J} , in the measure,

$$d\Omega = \frac{d\alpha_1}{\alpha_1} \frac{d\alpha_2}{\alpha_2} \dots \frac{d\alpha_m}{\alpha_m} \mathcal{J}^{\mathcal{N}-4} \cdot \delta(C \cdot Z). \quad (1.21)$$

This modification arises when passing from vertex-variables to edge-variables and \mathcal{J} is defined as the determinant of the adjacency matrix A_{ij} of the graph

$$\mathcal{J} = \det(1 - A). \quad (1.22)$$

The entries of A are given by,

$$A_{ij} = \text{weight of the directed edge } i \rightarrow j \text{ (if any)}. \quad (1.23)$$

If there is a collection of closed orbits bounding “faces” f_i , with *disjoint* pairs (f_i, f_j) , disjoint triples (f_i, f_j, f_k) etc., then the Jacobian \mathcal{J} can be expressed as,

$$\mathcal{J} = 1 + \sum_i f_i + \sum_{\substack{\text{disjoint} \\ \text{pairs } i,j}} f_i f_j + \sum_{\substack{\text{disjoint} \\ \text{triples } i,j,k}} f_i f_j f_k + \dots, \quad (1.24)$$

where each “face” f_i denotes the product of edge-variables along that orbit,

$$f_i = \prod_{r \in \text{closed orbit}_i} \alpha_r. \quad (1.25)$$

This factor cancels in $\mathcal{N} = 4$ sYM but in the case of lower supersymmetries it is present. For further details, we refer the reader directly to [12], Sec. 14. Here we included a brief discussion of \mathcal{J} as it will play a role in our gravity formulas later.

1.3 Hidden properties of $\mathcal{N} = 4$ sYM amplitudes

The Grassmannian formulation of on-shell diagrams make several important properties of scattering amplitudes in planar $\mathcal{N} = 4$ sYM completely manifest. The Yangian symmetry [31] is realized as positivity preserving diffeomorphisms [12], and the recursion relations (1.1) make manifest that it is also present in tree-level amplitudes and the loop integrands. The loop integration breaks the Yangian symmetry due to the presence of IR-divergencies [32] and all known regulators would break it as well. There is an on-going search for a new regulator which would preserve the Yangian using integrability techniques [33–36].

The other important property which is inherited in the formula (1.16) is the presence of logarithmic singularities only. This property is much stronger than just the

presence of single poles since we require $\frac{dx}{x}$ behavior near any pole in the cut structure. Each on-shell diagram is given by a $d \log$ form ($d \log x \equiv \frac{dx}{x}$) in terms of edge variables multiplied by a set of delta functions (1.16). One can solve for α_k in terms of external momenta and off-shell loop momenta, and the full integrand can be written as

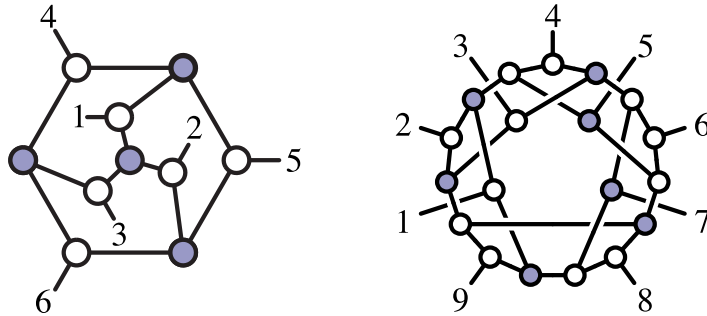
$$d\mathcal{I} = \sum_j d \log f_j^{(1)} d \log f_j^{(2)} d \log f_j^{(3)} \dots d \log f_j^{(4L)} \delta(C_j^* \cdot \tilde{\eta}) \quad (1.26)$$

where the $f_j^{(k)}$ depend both on external and internal momenta and C_j is the Grassmannian matrix with α_k substituted for. This representation of the loop integrand is very closely connected to the maximal transcendentality of $\mathcal{N} = 4$ planar amplitudes [12, 37–39]. For $k \leq 4$ the fermionic delta function does not depend on the loop momenta and the representation (1.26) can in principle be integrated directly so that one can obtain the final result in terms of polylogarithms [40–46]. For $k > 4$ the loop momenta are present in the fermionic delta function and the result is not a $d \log$ form in momentum space, but it still is in terms of edge variables. This gives rise to elliptic functions after integration which suggests that our notion of $d \log$ forms and transcendentality should be generalized to include these cases.

Finally, the on-shell diagrams make another important property completely manifest and that is the absence of poles at infinity [12]. In other words, the loop integrand in planar $\mathcal{N} = 4$ sYM as well as individual on-shell diagrams never generate a singularity which would correspond to sending the loop momentum to infinity, $\ell \rightarrow \infty$. This is a consequence of dual conformal symmetry and the representation of on-shell diagrams (and loop integrand) makes that manifest when using momentum twistor variables.

2 Non-planar on-shell diagrams

On-shell diagrams are well defined for any Quantum Field Theory with fundamental three point amplitudes and do not rely on the planarity of graphs. We can consider an arbitrary bi-colored graph with three-point vertices,



and define the on-shell function as the corresponding product of three-point amplitudes evaluated at specific on-shell kinematics dictated by the graph.

To each diagram we can associate a point in the Grassmannian, represented by the matrix C . This identification uses the rules explained in the previous section: associate variables with edges α_k , choose a perfect orientation and calculate the entries of the C -matrix using Eq. (1.12). If the diagram is planar and the edge variables are chosen real and with definite sign, we obtain a cell in the positive Grassmannian $G_+(k, n)$, in other cases we end up in some cell in a generic Grassmannian $G(k, n)$.

In general, we want to associate a form $d\Omega$ which reproduces the on-shell function given by the product of three point amplitudes,

$$d\Omega = df(\alpha_k) \delta(C \cdot Z) \quad (2.1)$$

where the measure $df(\alpha_k)$ depends on the theory while the delta function $\delta(C \cdot Z)$ only depends on the diagram and external kinematics. Therefore the problem naturally splits into two parts: finding the measure $df(\alpha_k)$ and the C -matrix. While the C -matrix associated to a given on-shell diagram can be found using Eq. (1.12), the classification of all possible non-planar diagrams and their associated particular subspace in $G(k, n)$ represent an important problem. For the case of MHV leading singularities the answer was given in [47] but understanding more general cases is a part of ongoing research [48].

For a generic Quantum Field Theory the measure $df(\alpha_k)$ associated with a given diagram is not known. However, for the case of Yang-Mills theory the answer has been worked out in [12] and turns out to be surprisingly simple,

$$d\Omega = \frac{d\alpha_1}{\alpha_1} \frac{d\alpha_2}{\alpha_2} \dots \frac{d\alpha_m}{\alpha_m} \mathcal{J}^{\mathcal{N}-4} \cdot \delta(C \cdot Z). \quad (2.2)$$

The \mathcal{J} -factor is given by the determinant of the adjacency matrix (1.23) and the singularities coming from this part of the measure are closely related to the UV-sector of the theory. In $\mathcal{N} = 4$ sYM this term is absent and we get a pure $d \log$ -form. From the discussion so far it is clear that writing the form (2.2) did not depend on the planarity of the diagram so that the formula is identical to (1.16) described in the planar sector. The goal of this section is to extend the knowledge of the Grassmannian formulation beyond the Yang-Mills case and find the analogue of (2.2) for gravity on-shell diagrams.

2.1 First look: MHV leading singularities

The leading singularities are reduced on-shell diagrams ($n_\delta = 0$) associated with on-shell functions Ω (rather than forms) and they represent codimension $4L$ cuts of loop

amplitudes. The simplest leading singularities are of MHV-type. In planar $\mathcal{N} = 4$ sYM they are all equal to the MHV tree-level amplitude given by the Parke-Taylor factor,

$$\text{PT}(123\dots n) = \frac{1}{\langle 12 \rangle \langle 23 \rangle \langle 34 \rangle \dots \langle n1 \rangle}. \quad (2.3)$$

Beyond the planar limit all MHV leading singularities must be holomorphic functions $F(\lambda)$ [14]. Furthermore, it was shown in [47] that all MHV leading singularities can be decomposed into linear combinations of Parke-Taylor factors with different orderings σ ,

$$\Omega = \sum_{\sigma} c_{\sigma} \text{PT}(\sigma_1 \sigma_2 \dots \sigma_n) \quad \text{where} \quad c_{\sigma} = \pm 1, 0. \quad (2.4)$$

This representation makes manifest the fact that all singularities are logarithmic as each Parke-Taylor factor behaves like $\frac{1}{x}$ near any singularity and one can infer the existence of the logarithmic form directly from the expression (2.4). Following the same logic, it is very natural to look at the MHV leading singularities in $\mathcal{N} = 8$ SUGRA and study their expressions in more detail.

Gluing together three-point amplitudes we find some suggestive expressions for a few simple on-shell diagrams (dropping the overall (super-) momentum conserving δ -functions in $\mathcal{N} = 8$ SUGRA $\delta^4(\lambda \cdot \tilde{\lambda}) \delta^{16}(\lambda \cdot \tilde{\eta})$),

$$\frac{[13][24]}{\langle 12 \rangle \langle 13 \rangle \langle 14 \rangle \langle 23 \rangle \langle 24 \rangle \langle 34 \rangle}$$

$$\frac{[12][23][45]^2}{\langle 12 \rangle \langle 13 \rangle \langle 15 \rangle \langle 23 \rangle \langle 34 \rangle \langle 45 \rangle}$$

$$\frac{[12][23][45]^2}{\langle 12 \rangle \langle 14 \rangle \langle 15 \rangle \langle 23 \rangle \langle 34 \rangle \langle 35 \rangle}$$

From these examples one could conjecture that all poles $\langle ij \rangle$ are linear and the numerator involves only anti-holomorphic brackets $[ij]$. However, looking at more complicated diagrams we learn that this is not the case and one gets both more complicated numerators and higher degree poles in the denominator.

$$\frac{\langle 5|Q_{16}|2\rangle\langle 2|Q_{34}|5\rangle[16]^2[34]^2}{\langle 12\rangle\langle 23\rangle\langle 34\rangle\langle 45\rangle\langle 56\rangle\langle 61\rangle\langle 25\rangle^2} \quad \frac{[23]^2\langle 1|Q_{23}|4\rangle\langle 4|Q_{23}|1\rangle\langle 1|Q_{67}|5\rangle\langle 1|Q_{57}|6\rangle\langle 4|Q_{56}|7\rangle^2}{\langle 14\rangle^3\langle 12\rangle\langle 15\rangle\langle 17\rangle\langle 23\rangle\langle 34\rangle\langle 45\rangle\langle 46\rangle\langle 56\rangle\langle 67\rangle}$$

Analyzing the data more closely, especially looking at the on-shell solutions for the momenta of the internal edges, one can make the following statement:

On-shell diagram vanishes if three momenta in a white vertex are collinear.

Concretely, the white vertex already enforces the λ 's to be proportional. If, on top of that, the $\tilde{\lambda}$'s become collinear as well (which implies the collinearity of momenta) the on-shell diagram vanishes. Interestingly, each factor in the numerator of the on-shell function exactly corresponds to such a condition which is why the number of factors in the numerators equals the number of white vertices in a given MHV on-shell diagram.

Taking a closer look at the denominator of the expressions one realizes that all factors which correspond to erasing edges from the on-shell diagram (by sending the momentum of that edge to zero) are single poles. In contrast, all higher poles (and some single poles) correspond to sending the momenta of an internal loop to infinity. Such poles are completely absent in the $\mathcal{N} = 4$ sYM case – this is related to the statement of no poles at infinity [49–51] – but in gravity they are present.

To clarify some of these statements, we discuss a concrete example and analyze the following on-shell diagram,

$$\begin{aligned} \ell_1 &= \frac{\lambda_1 Q_{12} \cdot \lambda_3}{\langle 13 \rangle}, & \ell_2 &= \frac{\lambda_5 Q_{12} \cdot \lambda_3}{\langle 35 \rangle}, \\ \ell_1 - 1 &= \frac{\langle 23 \rangle}{\langle 13 \rangle} \lambda_1 \tilde{\lambda}_2, & \ell_2 - 5 &= \frac{\langle 34 \rangle}{\langle 35 \rangle} \lambda_5 \tilde{\lambda}_4, \\ \ell_1 - Q_{12} &= \frac{\langle 12 \rangle}{\langle 13 \rangle} \lambda_3 \tilde{\lambda}_2, & \ell_2 - Q_{45} &= \frac{\langle 45 \rangle}{\langle 35 \rangle} \lambda_3 \tilde{\lambda}_4, \\ \ell_1 - Q_{123} &= \frac{\lambda_3 Q_{23} \cdot \lambda_1}{\langle 13 \rangle}, & \ell_1 + \ell_2 &= \frac{\langle 15 \rangle}{\langle 13 \rangle \langle 35 \rangle} \lambda_3 Q_{12} \cdot \lambda_3. \end{aligned}$$

$$\Omega = \frac{[12][23][45]^2}{\langle 12 \rangle \langle 13 \rangle \langle 15 \rangle \langle 23 \rangle \langle 34 \rangle \langle 45 \rangle} . \quad (2.5)$$

As explained above, most of the poles $\langle ij \rangle$ correspond to erasing edges in the on-shell diagram which is equivalent to setting the internal momentum of that edge to zero. In our example $\langle 13 \rangle$ corresponds to a pole at infinity and on this pole, all momenta associated with this loop blow up. Finally, let's look at the structure of the numerator. Focusing on the white vertex adjacent to external leg 1, the respective on-shell solutions for ℓ_1 and $\ell_1 - p_1$ as well as the external leg become collinear when $[12] = 0 \Rightarrow \tilde{\lambda}_2 \sim \tilde{\lambda}_1$, $\ell_1 \xrightarrow{[12] \rightarrow 0} \sim \lambda_1 \tilde{\lambda}_1$, $\ell_1 - p_1 \xrightarrow{[12] \rightarrow 0} \sim \lambda_1 \tilde{\lambda}_1$. As noted earlier, the gravity on-shell form vanishes in this limit due to the factor $[12]$ in the numerator. For the remaining white vertices, a similar analysis recovers all other square brackets $[ij]$ in the numerator of the gravity form (2.5).

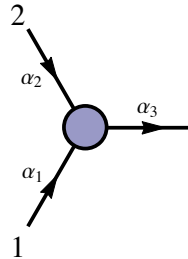
We can take these observations as a starting point in the search for the Grassmannian formulation of gravity on-shell diagrams. We learned that on-shell diagrams can have multiple poles associated with poles at infinity, and importantly the numerator factor must capture the curious collinear behavior observed above.

2.2 Three point amplitudes with spin s

The most natural starting point for a Grassmannian representation of gravity on-shell diagrams focuses on the atomic building blocks, the three-point amplitudes, first. We start with a maximally supersymmetric theory of particles with spin s . In that case, the amount of supersymmetry is given by $\mathcal{N} = 4s$. As noted before, in massless theories, the elementary three-point amplitudes are completely fixed by their little group weight to all orders in perturbation theory (up to an overall constant). In particular, the three-point MHV-amplitude for spin s particles is given by,

$$A_3^{(2)} = \frac{\delta^4(P) \delta^{2\mathcal{N}}(Q)}{\langle 12 \rangle^s \langle 23 \rangle^s \langle 31 \rangle^s} . \quad (2.6)$$

The on-shell diagram for this amplitude is just a single black vertex to which we can give a perfect orientation in exactly the same manner as for $\mathcal{N} = 4$ sYM discussed in section 1.2. We can use exactly the same rules from before to write the C -matrix,



$$C = \begin{pmatrix} 1 & 0 & \alpha_1 \alpha_3 \\ 0 & 1 & \alpha_2 \alpha_3 \end{pmatrix} . \quad (2.7)$$

Here we purposely do not choose any $GL(1)_v$ gauge fixing in the vertex because gauge-independence will be one of our criteria for finding the correct formula. The first step towards the Grassmannian representation of (2.6) is to write the linearized delta functions which have a very similar form to (1.17),

$$\delta^{(2 \times 2)}(C \cdot \tilde{\lambda}) \delta^{(1 \times 2)}(C^\perp \cdot \lambda) \delta^{(2 \times \mathcal{N})}(C \cdot \tilde{\eta}) = \frac{1}{\alpha_3^2 \langle 12 \rangle^{\mathcal{N}-1}} \delta^{(4)}(P) \delta^{(2\mathcal{N})}(\mathcal{Q}). \quad (2.8)$$

Using the two bosonic delta-functions from $\delta^{(1 \times 2)}(C^\perp \cdot \lambda)$, we can solve for two of the auxiliary α_k variables,

$$\alpha_1 = \frac{\langle 23 \rangle}{\alpha_3 \langle 12 \rangle}, \quad \alpha_2 = \frac{\langle 13 \rangle}{\alpha_3 \langle 12 \rangle}. \quad (2.9)$$

The general form of the Grassmannian representation of (2.6), for which the measure depends only on the α_k -variables and is permutation invariant in all three legs, is

$$d\Omega_\sigma = \frac{d\alpha_1}{\alpha_1^\sigma} \frac{d\alpha_2}{\alpha_2^\sigma} \frac{d\alpha_3}{\alpha_3^\sigma} \delta^{(2 \times 2)}(C \cdot \tilde{\lambda}) \delta^{(1 \times 2)}(C^\perp \cdot \lambda) \delta^{(2 \times \mathcal{N})}(C \cdot \tilde{\eta}), \quad (2.10)$$

for some integer σ . We can plug (2.8) and (2.9) into (2.10) to get

$$d\Omega_\sigma = \frac{d\alpha_3}{\alpha_3^{2-\sigma}} \cdot \frac{\delta^{(4)}(P) \delta^{(2\mathcal{N})}(\mathcal{Q})}{\langle 12 \rangle^{\mathcal{N}-1-2\sigma} \langle 23 \rangle^\sigma \langle 31 \rangle^\sigma}. \quad (2.11)$$

This expression must be permutation invariant in $\langle 12 \rangle$, $\langle 23 \rangle$, $\langle 31 \rangle$ and independent of the gauge-choice for α_3 . In order to ensure $GL(1)$ -invariance, $\frac{d\alpha_3}{\alpha_3}$ has to factor out as the volume of $GL(1)$ -transformations. These two requirements leave us with a unique choice: $\sigma = s = 1$ which corresponds to $\mathcal{N} = 4$ sYM with the logarithmic measure. Of course, one can also make a special choice, $\alpha_3 = \frac{1}{\langle 12 \rangle}$ so that $\alpha_1 = \langle 23 \rangle$, $\alpha_2 = \langle 13 \rangle$, which allows us to write any three point amplitude (2.6) using edge variables only. But our goal is to find a form which is independent of any such choices. Consequently, the form (2.10) is not able to reproduce the gravity or any higher spin three-point amplitude.

The natural modification of the form (2.10) involves some dimensionful, permutation invariant object Δ . The $\delta(C^\perp \cdot \lambda)$ allows us to relate $\alpha_1 \lambda_1 + \alpha_2 \lambda_2 + \frac{1}{\alpha_3} \lambda_3 = 0$ which we use in the definition of Δ as follows,

$$\Delta \equiv \langle AB \rangle = \langle BE \rangle = \langle EA \rangle \quad \text{where} \quad A = \alpha_1 \lambda_1, \quad B = \alpha_2 \lambda_2, \quad E = \frac{1}{\alpha_3} \lambda_3. \quad (2.12)$$

Note that this object has exactly the property suggested by our study of MHV leading singularities: it vanishes when all three momenta are collinear. Now we consider a form

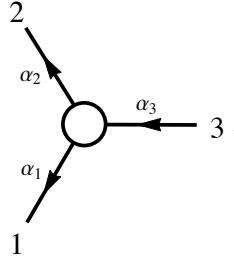
$$d\Omega = \frac{\Delta^\rho \cdot d\alpha_1 d\alpha_2 d\alpha_3}{\alpha_1^{\sigma_1} \alpha_2^{\sigma_2} \alpha_3^{\sigma_3}} \delta^{(2 \times 2)}(C \cdot \tilde{\lambda}) \delta^{(1 \times 2)}(C^\perp \cdot \lambda) \delta^{(2 \times \mathcal{N})}(C \cdot \tilde{\eta}). \quad (2.13)$$

Repeating the same exercise that led to (2.11) by solving for edge variables, converting the delta functions, imposing permutation invariance and the independence on α_3 uniquely fixes $\rho = s - 1$ and $\sigma_1 = \sigma_2 = \sigma_3 = 2s - 1$. The modified form becomes,

$$d\Omega_s = \frac{\Delta^{s-1} \cdot d\alpha_1 d\alpha_2 d\alpha_3}{\alpha_1^{2s-1} \alpha_2^{2s-1} \alpha_3^{2s-1}} \delta^{(2 \times 2)}(C \cdot \tilde{\lambda}) \delta^{(1 \times 2)}(C^\perp \cdot \lambda) \delta^{(2 \times \mathcal{N})}(C \cdot \tilde{\eta}) \quad (2.14)$$

which is a Grassmannian representation of (2.6). We would find the same unique solution even if we consider $\Delta = \langle 12 \rangle$ or any other function of $\alpha_1, \alpha_2, \alpha_3$ and $\langle 12 \rangle$ ($\langle 23 \rangle$ and $\langle 13 \rangle$ are proportional to $\langle 12 \rangle$ and α 's). Note that this formula is well defined for all integer spins s and maximal supersymmetry $\mathcal{N} = 4s$. In particular, for $s = 1$ it reproduces the logarithmic form of $\mathcal{N} = 4$ sYM.

There is an analogous Grassmannian representation for the $\overline{\text{MHV}}$ ($k = 1$) three-point amplitudes,



$$C = \begin{pmatrix} \alpha_1 \alpha_3 & \alpha_2 \alpha_3 & 1 \end{pmatrix}. \quad (2.15)$$

which can be encoded by the form,

$$d\tilde{\Omega}_s = \frac{\tilde{\Delta}^{s-1} \cdot d\alpha_1 d\alpha_2 d\alpha_3}{\alpha_1^{2s-1} \alpha_2^{2s-1} \alpha_3^{2s-1}} \delta^{(1 \times 2)}(C \cdot \tilde{\lambda}) \delta^{(2 \times 2)}(C^\perp \cdot \lambda) \delta^{(1 \times \mathcal{N})}(C \cdot \tilde{\eta}) \quad (2.16)$$

where $\tilde{\Delta} = [AB] = [BE] = [EA]$ with $A = \alpha_1 \tilde{\lambda}_1$, $B = \alpha_2 \tilde{\lambda}_2$ and $E = \frac{1}{\alpha_3} \tilde{\lambda}_3$.

2.3 Grassmannian formula

Equipped with the Grassmannian representation of the three-point amplitudes (2.14) and (2.16), we can write the Grassmannian representation for any spin s on-shell diagram. Much like in $\mathcal{N} = 4$ sYM, using the amalgamation procedure [12] to glue the three-point vertices into larger diagrams, we write the form in terms of edge variables,

$$d\Omega_s = \Gamma \cdot \frac{d\alpha_1 d\alpha_2 \dots d\alpha_d}{\alpha_1^{2s-1} \alpha_2^{2s-1} \dots \alpha_d^{2s-1}} \cdot \prod_{b \in B_v} \Delta_b^{s-1} \cdot \prod_{w \in W_v} \tilde{\Delta}_w^{s-1} \quad (2.17)$$

$$\times \mathcal{J}^{\mathcal{N}-4} \cdot \delta^{(k \times 2)}(C \cdot \tilde{\lambda}) \delta^{((n-k) \times 2)}(C^\perp \cdot \lambda) \delta^{(k \times \mathcal{N})}(C \cdot \tilde{\eta})$$

where Γ denotes any color factor/coupling constant associated with the diagram. The products of Δ_b and $\tilde{\Delta}_w$ are associated with the set of black (B_v) and white (W_v)

vertices respectively. They can be easily calculated using edge variables and external spinor-helicity variables. We are going to show some explicit examples in section 3.

Note that the Jacobian factor \mathcal{J} is the same as for $\mathcal{N} < 4$ sYM on-shell diagrams (1.22). The reason is that it originates from rewriting the (super-)momentum conserving delta functions in the linearized form using the C -matrix. In particular, it does not depend on the measure $df(\alpha_k)$ in (2.1) and therefore is the same for theories of arbitrary spin and number of supersymmetries. However, depending on the number of fermionic delta functions related to the amount of supersymmetry \mathcal{N} , the respective power $\mathcal{J}^{\mathcal{N}-4}$ changes and for $\mathcal{N} = 4$ always cancels. While the formula has been originally derived for $\mathcal{N} = 4s$ it is actually valid for any s and any \mathcal{N} , so it also captures theories with lower supersymmetries. The reason is that \mathcal{J} comes from solving the delta functions in the gluing three point vertices and also depends on the number supersymmetries, not the measure for a given theory.

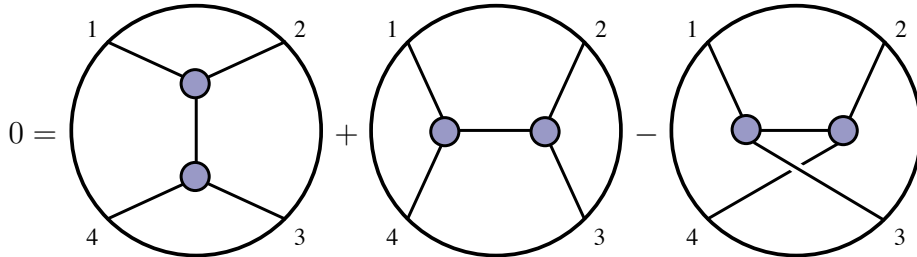
Before proceeding further, note that the on-shell diagrams for spin $s > 2$ make perfect sense as they are obtained from gluing elementary three point amplitudes together –which in turn are well defined. However, in Minkowski space, we know that there are no consistent long range forces mediated by spin $s > 2$ particles [52, 53]. From the point of on-shell diagrams, we can see that $s = 1, 2$ are special if we look at the identity moves on on-shell diagrams. There are two moves satisfied by planar on-shell diagrams: the square move (1.6) and merge-expand (1.5). These moves leave invariant the cell in the positive Grassmannian $G_+(k, n)$ as well as the logarithmic form $d\Omega$ which calculates the value of the on-shell diagram in $\mathcal{N} = 4$ sYM theory.

The content of the first move is the parity symmetry of a four point amplitude, and it does not really depend on planarity. Indeed, calculating the four point on-shell diagram (1.11)(a) we find that for general s it is equal to

$$\Omega_s = \left(\frac{[12]}{\langle 34 \rangle} \right)^{s-1} \cdot \frac{\delta^{(4)}(P) \delta^{(2\mathcal{N})}(\mathcal{Q})}{\langle 12 \rangle \langle 23 \rangle \langle 34 \rangle \langle 41 \rangle} \quad (2.18)$$

which is indeed invariant under the parity flip due to the totally crossing symmetric prefactor.

The merge-expand move gets modified beyond the planar limit. In fact, it is not a two-term relation (1.5) but now involves a third (non-planar) contribution,



Calculating all three diagrams either by gluing three point amplitudes or using the Grassmannian formula (2.17) we find that the invariance under this move requires

$$\Gamma_s(\langle 12 \rangle \langle 34 \rangle)^{s-1} + \Gamma_t(\langle 14 \rangle \langle 23 \rangle)^{s-1} = \Gamma_u(\langle 13 \rangle \langle 24 \rangle)^{s-1} \quad (2.19)$$

where Γ_k are the group factors for s -, t - and u -channels. There are only two solutions to this equation: Either $s = 1$ and $\Gamma_s + \Gamma_t = \Gamma_u$ which is nothing but the Jacobi identity for the color factors $\Gamma_s = f^{12a} f^{34a}$, $\Gamma_t = f^{14a} f^{23a}$, $\Gamma_u = f^{13a} f^{24a}$. Here we easily recognize $\mathcal{N} = 4$ sYM. The other option for which the merge-expand move holds is $s = 2$ and $\Gamma_s = \Gamma_t = \Gamma_u$ (and equal to some constant) due to the Shouten identity. This case corresponds to $\mathcal{N} = 8$ SUGRA. All higher spin cases (as well as for $s = 0$) are not consistent with the merge-expand move.

The merge-expand move is not an essential property of on-shell diagrams, indeed the $\mathcal{N} < 4$ SYM diagrams do not satisfy it. But for maximally supersymmetric theories it seems like a good guide when the theory is healthy. From now on, we will focus on the $s = 2$ case of $\mathcal{N} = 8$ SUGRA. For this theory, the Grassmannian representation becomes,

$$d\Omega = \frac{d\alpha_1 d\alpha_2 \dots d\alpha_d}{\alpha_1^3 \alpha_2^3 \dots \alpha_d^3} \prod_{b \in B_v} \Delta_b \prod_{w \in W_v} \tilde{\Delta}_w \quad (2.20)$$

$$\times \mathcal{J}^4 \cdot \delta^{(k \times 2)}(C \cdot \tilde{\lambda}) \delta^{((n-k) \times 2)}(C^\perp \cdot \lambda) \delta^{(k \times 8)}(C \cdot \tilde{\eta}) .$$

Note that a similar formula is valid for $\mathcal{N} < 8$ SUGRA subject to the simple replacement $\mathcal{J}^4 \rightarrow \mathcal{J}^{\mathcal{N}-4}$. In these cases we also have to sum over all possible orientations of internal edges, in complete analogy to the Yang-Mills case.

3 Properties of gravity on-shell diagrams

In this section we are going to elaborate on the Grassmannian formula for gravity (2.20) obtained in the last section. We will show on examples how to use the formula to calculate particular on-shell diagrams and comment on their properties.

3.1 Calculating on-shell diagrams

After deriving the Grassmannian formulation for on-shell diagrams in $\mathcal{N} = 8$ SUGRA in an abstract setting, let's consider a few concrete examples to show that we can reproduce the correct values of the on-shell functions derived before. As a first non-trivial example, we consider a reduced on-shell diagram for five external particles. For the construction of the C -matrix, we chose a convenient perfect orientation. Of course, the final result will be independent of the particular choice. Since we were able to choose

a perfect orientation without any closed loops, the Jacobian factor \mathcal{J} in Eq. (1.22) from converting between vertex- and edge-variables is trivial, $\mathcal{J} = 1$.

In complete analogy to the Yang Mills case, we have used the $GL(1)_v$ -freedom from all vertices to gauge fix several of the edge-weights to 1. Starting from the gauge-fixed on-shell diagram, we can follow the same rules described in Sec. 1.2 to construct the boundary-measurement matrix C by summing over paths from sources to sinks and multiplying the edge weights along the path.

$$C = \begin{pmatrix} 1 & \alpha_1 + \alpha_2\alpha_6 & \alpha_6 & \alpha_3\alpha_6 & 0 \\ 0 & \alpha_5\alpha_6\alpha_2 & \alpha_5\alpha_6 & \alpha_4 + \alpha_3\alpha_5\alpha_6 & 1 \end{pmatrix} \quad (3.1)$$

The orthogonal matrix C^\perp is then given by,

$$C^\perp = \begin{pmatrix} -(\alpha_1 + \alpha_2\alpha_6) & 1 & 0 & 0 & -\alpha_5\alpha_6\alpha_2 \\ -\alpha_6 & 0 & 1 & 0 & -\alpha_5\alpha_6 \\ -\alpha_3\alpha_6 & 0 & 0 & 1 & -(\alpha_4 + \alpha_3\alpha_5\alpha_6) \end{pmatrix}. \quad (3.2)$$

We can use the $\delta^{(3 \times 2)}(C^\perp \cdot \lambda)$ delta-functions to solve for all edge variables α_i ,

$$\alpha_1 = \frac{\langle 23 \rangle}{\langle 13 \rangle}, \quad \alpha_2 = \frac{\langle 12 \rangle}{\langle 13 \rangle}, \quad \alpha_3 = \frac{\langle 45 \rangle}{\langle 35 \rangle}, \quad \alpha_4 = \frac{\langle 34 \rangle}{\langle 35 \rangle}, \quad \alpha_5 = \frac{\langle 13 \rangle}{\langle 35 \rangle}, \quad \alpha_6 = \frac{\langle 35 \rangle}{\langle 15 \rangle}. \quad (3.3)$$

Solving for all the α_i induces a Jacobian $J_{C^\perp, \lambda} = (\langle 35 \rangle^2 \langle 13 \rangle)^{-1}$. Plugging these solutions $\alpha_i = \alpha_i^*$ back into the remaining δ -functions, we find,

$$\delta^{(2 \times 2)}(C \cdot \tilde{\lambda}) = \langle 15 \rangle^2 \delta^4(\lambda \cdot \tilde{\lambda}), \quad \delta^{(2 \times \mathcal{N})}(C \cdot \tilde{\eta}) = \frac{1}{\langle 15 \rangle^{\mathcal{N}}} \delta^{2\mathcal{N}}(\lambda \cdot \tilde{\eta}). \quad (3.4)$$

As a quick sanity check, we can recover the $\mathcal{N} = 4$ sYM result,

$$\begin{aligned} d\Omega_{\mathcal{N}=4} &= \prod_{i=1}^6 \frac{d\alpha_i}{\alpha_i} \delta^{(2 \times 2)}(C \cdot \tilde{\lambda}) \delta^{(3 \times 2)}(C^\perp \cdot \lambda) \delta^{(2 \times 4)}(C \cdot \tilde{\eta}) \\ &= \text{PT}(12345) \delta^{(4)}(\lambda \cdot \tilde{\lambda}) \delta^{(2 \times 4)}(\lambda \cdot \tilde{\eta}) \end{aligned} \quad (3.5)$$

The only missing ingredient for the gravity result are the various Δ_b and $\tilde{\Delta}_w$ factors required in the definition of the measure (2.20). In order to calculate Δ_b and $\tilde{\Delta}_w$ the knowledge of the adjacent λ and $\tilde{\lambda}$ are required. Naively one could think that one has to solve for all internal momenta explicitly in order to construct the Δ 's and $\tilde{\Delta}$'s. However, the on-shell diagram knows about all relations between the internal λ 's and $\tilde{\lambda}$'s and the external kinematic data automatically. That is the point of constructing the C matrix using the paths and there are simple rules how to read off Δ_b and $\tilde{\Delta}_w$ directly from the diagram.

Let us first formulate the rule for the white vertices $\tilde{\Delta}_w$ which is defined as a contraction of two incoming $\tilde{\lambda}$ spinors in the vertex,

$$\tilde{\Delta}_w = [\tilde{\lambda}_A \tilde{\lambda}_B] \quad (3.6)$$

This naively depends on the split of the internal momenta $p_I = \lambda_I \tilde{\lambda}_I$ into spinors as well as the choice which two of the $\tilde{\lambda}$'s to pick. However the on-shell diagram gives us the correct split automatically similar to how it is provided in the delta functions (2.20). Furthermore, since the $\tilde{\lambda}$ -spinor is conserved in each vertex –which is exactly the purpose of the linearized delta functions– it does not matter which two we pick. Following the rules used in the construction of the C -matrix, we choose two of the outgoing $\tilde{\lambda}$. Then we track each of them back to the external momenta following the rules:

If we hit a black vertex we follow the path, if we hit a white vertex we sum over both paths. At each step we multiply by the edge variables on the way.

Note that this is exactly how the C -matrix is constructed, just that there we start with the incoming external legs rather than the legs attached to an internal vertex. In case of closed internal loops, it might be necessary to sum a geometric series as in the construction of the C -matrix.

The rule for Δ_b is similar, it is a contraction of two λ spinors,

$$\Delta_b = \langle \lambda_A \lambda_B \rangle. \quad (3.7)$$

Now we choose the two incoming arrows in the black vertex and trace them back to external legs going against the arrows rather than following the arrows. This can be trivially understood from the linearized delta functions, the $\tilde{\lambda}$ spinors are coupled to the C -matrix but the λ spinors are coupled to the C^\perp which can be thought of as the C -matrix for on-shell diagrams where all black and white vertices as well as all arrows are flipped.

In our example (3.1), let us start with the white vertices. Following the arrows from the vertex W_1 we leave the diagram via the *sinks*, and the spinors are,

$$\tilde{\lambda}_A = \alpha_4 \tilde{\lambda}_4, \quad \tilde{\lambda}_B = \alpha_5 \alpha_6 (\alpha_3 \tilde{\lambda}_4 + \tilde{\lambda}_3 + \alpha_2 \tilde{\lambda}_2) \quad (3.8)$$

corresponding to $\tilde{\Delta}_1$,

$$\tilde{\Delta}_1 = [\tilde{\lambda}_A \tilde{\lambda}_B] = -\alpha_4 \alpha_5 \alpha_6 ([34] + \alpha_2 [24]) \quad (3.9)$$

Similarly, for the other vertices we get,

$$\tilde{\Delta}_2 = \alpha_1 (\alpha_3 [24] + [23]), \quad \tilde{\Delta}_3 = \alpha_2 [23], \quad \tilde{\Delta}_4 = \alpha_3 ([34] + \alpha_2 [24]). \quad (3.10)$$

For the black vertices we just go against the arrows and leave the diagram via the *sources*.

$$\Delta_1 = \alpha_3 \alpha_4 \alpha_6 \langle 15 \rangle, \quad \Delta_2 = \alpha_5 \langle 15 \rangle, \quad \Delta_3 = \alpha_1 \alpha_2 \alpha_5 \alpha_6 \langle 15 \rangle \quad (3.11)$$

Collecting all terms in (2.20) our formula for the on-shell diagram is (omitting $d\alpha_k$)

$$d\Omega = \frac{([23] + \alpha_3 [24])^2 ([34] + \alpha_2 [34]) [23] \langle 15 \rangle^3}{\alpha_1 \alpha_2 \alpha_3 \alpha_4} \delta^{(2 \times 2)}(C \cdot \tilde{\lambda}) \delta^{(3 \times 2)}(C^\perp \cdot \lambda) \delta^{(2 \times 8)}(C \cdot \tilde{\eta}). \quad (3.12)$$

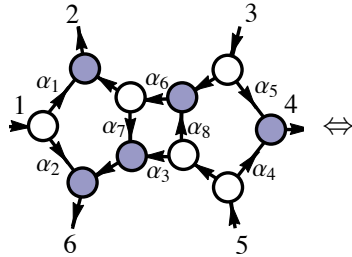
Substituting the solutions for the edge variables (3.3), converting the δ -functions and including the Jacobians reproduces the same gravity result (2.5) we obtained from gluing three-point amplitudes directly,

$$d\Omega = \frac{[12][23][45]^2}{\langle 12 \rangle \langle 23 \rangle \langle 34 \rangle \langle 45 \rangle \langle 51 \rangle \langle 13 \rangle} \delta^4(\lambda \cdot \tilde{\lambda}) \delta^{16}(\lambda \cdot \tilde{\eta}). \quad (3.13)$$

Note that the formula (3.12) has only single poles in α_k in contrast to the cubic poles in the general form (2.20). We will expand on this point later in this section.

3.2 More examples

So far we have mostly considered simple MHV examples. Here we would like to stress that our Grassmannian formulation for gravity on-shell diagrams is not restricted to the MHV sector but works for arbitrary k as well. To illustrate this point, let us consider a simple NMHV on-shell diagram,



$$C = \begin{pmatrix} 1 & \alpha_1 & 0 & 0 & 0 & \alpha_2 \\ 0 & \alpha_6 & 1 & \alpha_5 & 0 & \alpha_6 \alpha_7 \\ 0 & \alpha_6 \alpha_8 & 0 & \alpha_4 & 1 & \alpha_3 + \alpha_6 \alpha_7 \alpha_8 \end{pmatrix}$$

$$C^\perp = \begin{pmatrix} -\alpha_1 & 1 & -\alpha_6 & 0 & -\alpha_6 \alpha_8 & 0 \\ 0 & 0 & -\alpha_5 & 1 & -\alpha_4 & 0 \\ -\alpha_2 & 0 & -\alpha_6 \alpha_7 & 0 & -(\alpha_3 + \alpha_6 \alpha_7 \alpha_8) & 1 \end{pmatrix}.$$

Here we are going to have additional fermionic δ -functions which exactly give us eight extra powers of $\tilde{\eta}$ required for NMHV on-shell functions. Solving the bosonic δ -functions for the edge variables we find,

$$\alpha_1 = -\frac{[16]}{[26]}, \quad \alpha_2 = \frac{[12]}{[26]}, \quad \alpha_3 = \frac{s_{345}}{\langle 5|Q_{345}|6\rangle}, \quad \alpha_4 = \frac{\langle 34\rangle}{\langle 35\rangle}, \quad \alpha_5 = \frac{\langle 45\rangle}{\langle 35\rangle},$$

$$\alpha_6 = \frac{\langle 5|Q_{345}|6\rangle}{\langle 35\rangle[26]}, \quad \alpha_7 = -\frac{\langle 5|Q_{345}|2\rangle}{\langle 5|Q_{345}|6\rangle}, \quad \alpha_8 = -\frac{\langle 3|Q_{345}|6\rangle}{\langle 5|Q_{345}|6\rangle}.$$

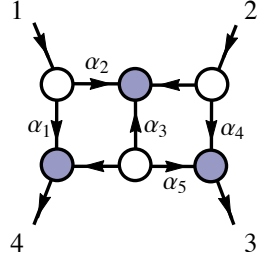
Converting the δ -functions,

$$\delta(C \cdot Z) = \frac{[26]\langle 35\rangle \prod_{i=1}^8 \delta(\alpha_i - \alpha_i^*)}{\langle 5|Q_{345}|6\rangle \langle 35\rangle^8 [26]^8} \delta^4(P) \delta^{16}(\mathcal{Q}) \delta^8([26]\tilde{\eta}_1 + [61]\tilde{\eta}_2 + [12]\tilde{\eta}_6), \quad (3.14)$$

and writing all numerator factors $\Delta_{b_i}, \tilde{\Delta}_{w_j}$ exactly as before, the on-shell function is,

$$d\Omega = \frac{\langle 12\rangle\langle 16\rangle[34][45] \delta^8([26]\tilde{\eta}_1 + [61]\tilde{\eta}_2 + [12]\tilde{\eta}_6)}{[12][26][61]s_{345}\langle 34\rangle\langle 45\rangle\langle 53\rangle\langle 5|Q_{345}|2\rangle\langle 3|Q_{345}|6\rangle} \delta^4(P) \delta^{16}(\mathcal{Q}). \quad (3.15)$$

As a further example, we can check that our Grassmannian formula for gravity on-shell diagrams also reproduces the correct result in cases where the graphs are non-reduced, i.e. contain additional degrees of freedom not localized by the bosonic δ -functions. The simplest case to consider is the following,



$$\Leftrightarrow \begin{aligned} C &= \begin{pmatrix} 1 & 0 & \alpha_3\alpha_4\alpha_5 & \alpha_1 + \alpha_2\alpha_3 \\ 0 & 1 & \alpha_4 + \alpha_3\alpha_5 & \alpha_3 \end{pmatrix} \\ C^\perp &= \begin{pmatrix} -\alpha_2\alpha_3\alpha_5 & -(\alpha_4 + \alpha_3\alpha_5) & 1 & 0 \\ -(\alpha_1 + \alpha_2\alpha_3) & -\alpha_3 & 0 & 1 \end{pmatrix}. \end{aligned}$$

Choosing α_1 to be the free parameter, we solve for the remaining edge-variables,

$$\alpha_2 = \frac{\langle 42\rangle - \alpha_1\langle 12\rangle}{\langle 14\rangle}, \quad \alpha_3 = \frac{\langle 14\rangle}{\langle 12\rangle}, \quad \alpha_4 = \frac{\langle 43\rangle - \alpha_1\langle 13\rangle}{\langle 42\rangle - \alpha_1\langle 12\rangle}, \quad \alpha_5 = \frac{\langle 32\rangle}{\langle 42\rangle - \alpha_1\langle 12\rangle}.$$

As a cross check, we can again look at the Yang–Mills result $d\Omega_{\text{YM}} = \frac{1}{\alpha_1\langle 12\rangle\langle 14\rangle\langle 23\rangle(\langle 43\rangle - \alpha_1\langle 13\rangle)}$, which agrees with the form found earlier in (1.4) once we identify $\alpha_1 \leftrightarrow -z$.

The gravity result can be obtained using our rules from the previous sections,

$$d\Omega = \frac{[24][23][41]}{\alpha_1\langle 12\rangle\langle 13\rangle\langle 23\rangle\langle 41\rangle(\langle 43\rangle - \alpha_1\langle 13\rangle)} \delta^4(P) \delta^{16}(\mathcal{Q}) \quad (3.16)$$

All previous examples were in the context of maximal supersymmetry. Here we will explicitly consider a non-supersymmetric case to demonstrate that our Grassmannian formula also holds there. Since the only difference to the maximally supersymmetric theory is the Jacobian \mathcal{J} for on-shell diagrams with a perfect orientation containing closed internal cycles (c.f. (2.20)), we look at the simplest diagrams,

$$C^{(a)} = \begin{pmatrix} \alpha_2 \alpha_3 \alpha_4 \delta_a & 1 & \alpha_2 \delta_a & 0 \\ \alpha_4 \delta_a & 0 & \alpha_4 \alpha_1 \alpha_2 \delta_a & 1 \end{pmatrix} \quad C^{(b)} = \begin{pmatrix} \beta_1 \delta_b & 1 & \beta_1 \beta_4 \beta_3 \delta_b & 0 \\ \beta_3 \beta_2 \beta_1 \delta_b & 0 & \beta_3 \delta_b & 1 \end{pmatrix}$$

As mentioned before, in order to obtain the correct result, we have to sum over all possible orientations of the internal loop which is why we include both diagrams. Introducing the usual short-hand notation for the geometric series $\delta_a = (1 - \alpha_1 \cdots \alpha_4)^{-1}$, $\delta_b = (1 - \beta_1 \cdots \beta_4)^{-1}$ and solving for the edge variables we find,

$$\delta(C^{(a)}, Z) = \frac{\langle 24 \rangle^4 \delta^4(P)}{\langle 12 \rangle^2 \langle 34 \rangle^2} \delta \left[\alpha_1 + \frac{\langle 23 \rangle}{\langle 13 \rangle} \right] \delta \left[\alpha_2 - \frac{\langle 13 \rangle}{\langle 12 \rangle} \right] \delta \left[\alpha_3 + \frac{\langle 14 \rangle}{\langle 13 \rangle} \right] \delta \left[\alpha_4 + \frac{\langle 13 \rangle}{\langle 34 \rangle} \right], \quad (3.17)$$

$$\delta(C^{(b)}, Z) = \frac{\langle 24 \rangle^4 \delta^4(P)}{\langle 14 \rangle^2 \langle 23 \rangle^2} \delta \left[\beta_1 - \frac{\langle 13 \rangle}{\langle 23 \rangle} \right] \delta \left[\beta_2 - \frac{\langle 21 \rangle}{\langle 13 \rangle} \right] \delta \left[\beta_3 - \frac{\langle 13 \rangle}{\langle 14 \rangle} \right] \delta \left[\beta_4 - \frac{\langle 34 \rangle}{\langle 13 \rangle} \right]. \quad (3.18)$$

We can easily find the respective numerators and Jacobians \mathcal{J} (1.22) required for our gravity formula (2.20),

$$N^{(a)} = \alpha_1^2 \alpha_3^2 s_{12}^2, \quad \mathcal{J}^{(a)} = 1 - \alpha_1 \alpha_2 \alpha_3 \alpha_4, \quad N^{(b)} = \beta_2^2 \beta_4^2 s_{14}^2, \quad \mathcal{J}^{(b)} = 1 - \beta_1 \beta_2 \beta_3 \beta_4,$$

to put everything together ($\mathcal{N} = 0 \Leftrightarrow \mathcal{J}^{-4}$),

$$d\Omega^{\mathcal{N}=0} = \frac{\langle 24 \rangle^4}{\langle 13 \rangle^4} \left(s_{12}^2 \frac{\langle 12 \rangle \langle 34 \rangle}{\langle 14 \rangle \langle 23 \rangle} \left[\frac{\langle 13 \rangle \langle 24 \rangle}{\langle 12 \rangle \langle 34 \rangle} \right]^{-4} + s_{14}^2 \frac{\langle 14 \rangle \langle 23 \rangle}{\langle 12 \rangle \langle 34 \rangle} \left[\frac{\langle 13 \rangle \langle 24 \rangle}{\langle 14 \rangle \langle 23 \rangle} \right]^{-4} \right) \delta^4(P) \quad (3.19)$$

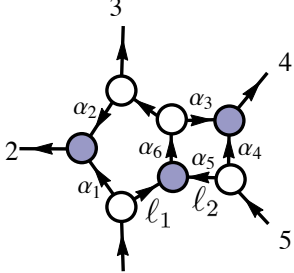
which agrees with the formula obtained by simply gluing three-point amplitudes together. This serves as a further verification of our Grassmannian formula for gravity on-shell diagrams (2.20).

3.3 Structure of singularities

There are two different types of singularities of on-shell diagrams. In terms of edge-variables, these are $\alpha_k \rightarrow 0$ or $\alpha_k \rightarrow \infty$ which correspond to either erasing edges or are

associated with poles at infinity when all on-shell momenta in a given loop are located at $\ell \rightarrow \infty$.

Let us show the different cases for the on-shell diagram discussed in previous subsections, and also calculated in section 3.1. when we first looked at gravity on-shell diagrams.



$$\begin{aligned}
\ell_1 &= \frac{\lambda_1}{\langle 13 \rangle} \frac{Q_{12} \cdot \lambda_3}{\langle 13 \rangle}, & \ell_2 &= \frac{\lambda_5}{\langle 35 \rangle} \frac{Q_{12} \cdot \lambda_3}{\langle 35 \rangle}, \\
\ell_1 - 1 &= \frac{\langle 23 \rangle}{\langle 13 \rangle} \lambda_1 \tilde{\lambda}_2, & \ell_2 - 5 &= \frac{\langle 34 \rangle}{\langle 35 \rangle} \lambda_5 \tilde{\lambda}_4, \\
\ell_1 - Q_{12} &= \frac{\langle 12 \rangle}{\langle 13 \rangle} \lambda_3 \tilde{\lambda}_2, & \ell_2 - Q_{45} &= \frac{\langle 45 \rangle}{\langle 35 \rangle} \lambda_3 \tilde{\lambda}_4, \\
\ell_1 - Q_{123} &= \frac{\lambda_3}{\langle 13 \rangle} \frac{Q_{23} \cdot \lambda_1}{\langle 13 \rangle}, & \ell_1 + \ell_2 &= \frac{\langle 15 \rangle}{\langle 13 \rangle \langle 35 \rangle} \lambda_3 Q_{12} \cdot \lambda_3.
\end{aligned}$$

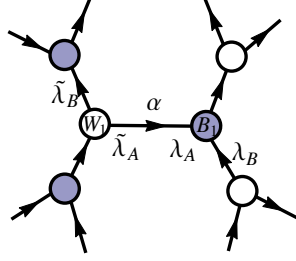
$$\alpha_1 = \frac{\langle 23 \rangle}{\langle 13 \rangle}, \quad \alpha_2 = \frac{\langle 12 \rangle}{\langle 13 \rangle}, \quad \alpha_3 = \frac{\langle 45 \rangle}{\langle 35 \rangle}, \quad \alpha_4 = \frac{\langle 34 \rangle}{\langle 35 \rangle}, \quad \alpha_5 = \frac{\langle 13 \rangle}{\langle 35 \rangle}, \quad \alpha_6 = \frac{\langle 35 \rangle}{\langle 15 \rangle}.$$

Here we can see that four of the edge variables, α_1 , α_2 , α_3 and α_4 , directly parametrize the momentum flow in a given edge. If we send one of them to zero, the zero momentum flow effectively erases that edge. Similarly, sending $\alpha_6 \rightarrow \infty$ erases the corresponding $(\ell_1 + \ell_2)$ -edge. Whether the location of the pole is at 0 or ∞ is determined by the orientation of the arrow on the edge, flipping the orientation of the arrow inverts the edge variable $\alpha_k \rightarrow \frac{1}{\alpha_k}$ and the location of the pole changes. Independent of the details of the orientation, the important statement is that all of the discussed edges are erasable by sending $\alpha_k \rightarrow 0$ or ∞ . Note that the edge corresponding to α_5 is not erasable. The reason is that if we tried to erase this edge, the remaining diagram would enforce both $[45] = \langle 13 \rangle = 0$ which imposes too many constraints. In fact, sending $\alpha_5 \rightarrow 0$ or ∞ blows up one of the loops with $\ell_1 \rightarrow \infty$ or $\ell_2 \rightarrow \infty$. The same happens if we set α_1 , α_2 , α_3 , α_4 to infinity or α_6 to zero. In the example above, we have already chosen a particular $GL(1)_v$ gauge-fixing, corresponding to the fact that some edge-variables are set to 1. For a different gauge-fixing we could analyze these edges as well, leading to the same set of erasable edges described above.

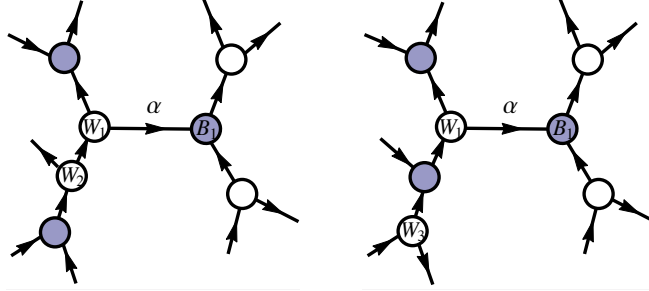
In the case of $\mathcal{N} = 4$ sYM theory the form is logarithmic in all edge variables independent whether an edge is erasable or not. Furthermore, the final expression does not contain any poles that send loop-momenta to infinity so that all singularities correspond to erasing edges only. This is an important distinction to $\mathcal{N} = 8$ SUGRA where poles at infinity do appear.

Let us investigate the properties of our Grassmannian form for gravity on-shell diagrams a little more closely. First, it is relatively easy to see that the form (2.20) has only linear poles for $\alpha_k \rightarrow 0$, when the corresponding edge is erasable. The denominator

contains the third power of this edge variable, α_k^3 but the numerator always generates two powers leaving only a single pole. We remove the erasable edge in the on-shell diagram for $\alpha_k \rightarrow 0$ if the arrow points from a white to a black vertex, while it is erased by $\alpha_k \rightarrow \infty$ if the arrow points from a black to a white vertex. The edges between same colored vertices are never removable.



The numerator for such subgraph is given by the products of Δ_b and $\tilde{\Delta}_w$. Based on our rules, we have $\Delta_{b_1} = \langle \lambda_A \lambda_B \rangle \sim \alpha$ and $\tilde{\Delta}_{w_1} = [\tilde{\lambda}_A \tilde{\lambda}_B] \sim \alpha$, while all other Δ_b and $\tilde{\Delta}_w$ do not depend on α . Therefore the numerator generates $\sim \alpha^2$. We can also consider a modification of the subgraph by adding another white vertex (or in general a chain of white vertices), or consider some more distant vertex and look if they can possibly generate additional α factors in the numerator,

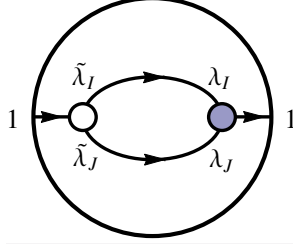


In both cases the numerator will have further α -dependence but in either situation, it will look like $\tilde{\Delta}_{w2}, \tilde{\Delta}_{w3} \sim \alpha(\dots) + (\dots)$ and the linearity of the pole in α is not changed. The argument for erasable edges would be similar when the arrow points from black to white vertex. The only difference is that we have to keep track of the pole $\alpha \rightarrow \infty$ but we would again find a linear pole only. Alternatively, we can take the same diagram and consider a different perfect orientation in which the arrow again points from white to black so that the pole is localized at zero. As a result, all poles corresponding to erasable edges are linear. This immediately implies that all higher

poles (including some simple poles) correspond to poles at infinity, when internal on-shell momenta in one or more loops are sent to infinity.

Bubbles

Let us comment on one important property of gravity on-shell diagrams which is a trivial consequence of the formula (2.20): any internal bubble **vanishes**. Let us consider a diagram with an internal bubble.



Independent of the rest of the diagram, the perfect orientation chosen and the directions of arrows, the numerator factors Δ_b and $\tilde{\Delta}_w$ vanish for both vertices separately. All $\tilde{\lambda}$'s in the black vertex are proportional, so are all λ 's in the white vertex, which implies that $\lambda_1 \sim \lambda_I \sim \lambda_J$ and $\tilde{\lambda}_1 \sim \tilde{\lambda}_I \sim \tilde{\lambda}_J$ and $\Delta_b = \tilde{\Delta}_w = 0$.

This fact will have dramatic consequences on properties of loop amplitudes. We will discuss them in greater detail in the next section. Furthermore, there is one interesting aspect related to vanishing bubbles: in planar $\mathcal{N} = 4$ sYM, the loop integrand is expressed in terms of on-shell diagrams containing bubbles. In fact, via equivalence moves, one can show that four bubbles built the four degrees of freedom of the off-shell loop momentum for each loop [12]. We do not have any recursion relations in the gravity case (as well as in $\mathcal{N} = 4$ sYM beyond the planar limit) but if such formulation exists, it must take this fact into account. In the planar case we could always use the identity moves to eliminate the bubble from the diagram in the form (see figure above). The non-planar identity moves for $\mathcal{N} = 8$ SUGRA (and also non-planar $\mathcal{N} = 4$ SYM) are different which might lead to a different role of bubbles in the loop integrand.

4 From on-shell diagrams to scattering amplitudes

In the last sections we initiated a detailed study of gravity on-shell diagrams and gave their Grassmannian representation. This formula (2.20) exhibited some interesting properties: (a) higher poles associated with sending internal momenta to infinity and (b) vanishing whenever three momenta in any vertex become collinear. As it was stressed several times, the on-shell diagrams represent cuts of loop integrands and they

contain a considerable amount of information about the structure of loop amplitudes themselves even though we do not yet know how to express the integrand directly in terms of on-shell diagrams. There are two obvious paths beyond the well-understood case of planar $\mathcal{N} = 4$ sYM theory: (i) going to lower supersymmetry or (ii) going non-planar. The recursion relations for planar non-supersymmetric Yang-Mills theory suffers from divergencies in the forward limit term. Resolving that problem is an active area of research [54] and it appears to be a question of properly defining the forward limit term in these theories rather than some fundamental obstruction.

The extension to non-planar theories, even with maximal supersymmetry, seems more difficult because it is not even clear which object should recurse in the first place. Beyond the planar limit we do not have global variables and loop momenta are normally associated with individual diagrams in the Feynman expansion, or its refined version using a set of integrals in the unitarity method. Therefore it is not clear how to associate the "loop-momentum" degrees of freedom with those in on-shell diagrams or how to cancel spurious poles. Making progress on this problem would certainly open doors to many new directions of research. However, even without having the recursion relations at hand, there is an immediate question one can ask:

Does the loop amplitude have the same properties as individual on-shell diagram?

This analysis was done in particular examples for amplitudes in full non-planar $\mathcal{N} = 4$ sYM theory and the answer is positive [49–51]. Additionally, many of the structures present in the planar limit seem to survive in non-planar amplitudes despite the absence of good kinematic variables. We review this progress in the next subsection and then motivated by this success we will test the properties found for gravity on-shell diagrams on explicit expressions for gravity amplitudes.

4.1 Non-planar $\mathcal{N} = 4$ sYM amplitudes

In the $\mathcal{N} = 4$ sYM case we are able to take the step to non-planar amplitudes. On one hand we have a detailed understanding of the planar sector of the theory and the properties of the amplitudes: logarithmic singularities, dual conformal [17, 55, 56] and Yangian [31] symmetries as well as the Amplituhedron [57] construction. On the other hand, we have the non-planar on-shell diagrams which have logarithmic singularities and for MHV leading singularities we even know that they are expressed in terms of planar ones.

All these ingredients lead to the following conjectures [49–51]:

- The loop amplitudes have only **logarithmic singularities**, as in the planar limit. For $k > 4$ (perhaps even for lower k) we expect the presence of elliptic cuts

but at least for $k = 2$ the logarithmic singularities must be present directly in momentum space.

- There are **no poles at infinity**. This was one of the consequence of the dual conformal symmetry of planar amplitudes, but also motivated by the observation about MHV leading singularities.

These conjectures were tested in [49–51] on the four-point amplitudes at two- and three-loops, and on the five-point amplitude at two-loops. These tests rely on a two-step process. First one constructs the basis of integrals \mathcal{I}_k with the above two properties (also with unit leading singularities) and second one expands the loop amplitudes in this basis. The correctness of the result is guaranteed by satisfying all unitarity cuts.

$$\mathcal{A} = \sum_k c_k \mathcal{I}_k \quad (4.1)$$

As was argued in [50, 51] this is a strong evidence for a new hidden symmetry (analogue of dual conformal symmetry) in the full $\mathcal{N} = 4$ sYM theory.

Finally, the step towards the geometric Amplituhedron-like construction was also made in [51]. The presence of logarithmic singularities only was one of the ingredients of the Amplituhedron where the $d \log$ forms can be thought of as volumes in the Grassmannian. Moreover, motivated by the work [58] it was checked that all coefficients c_k in (4.1) can be fixed only from vanishing cuts. This means that the full amplitude is fixed entirely by homogeneous conditions providing nontrivial evidence for an Amplituhedron-type geometric formulation.

Motivated by this success we can now turn to gravity and see what structures we can carry over from on-shell diagrams directly to the amplitude. In particular, we want to test two statements:

- All singularities are logarithmic unless it is a pole at infinity.
- The amplitude **vanishes** on all collinear cuts.

The first statement is motivated by the singularity structure of gravity on-shell diagrams described in Sec. 3.3. There, we saw that certain single poles correspond to erasable edges, and all higher poles are associated with sending internal momenta to infinity. The second statement is the crucial ingredient in the Grassmannian formula (2.20) and checking it for gravity amplitudes will be a main result of this section.

4.2 Gravity from Yang-Mills

The relation between scattering amplitudes in Yang-Mills theory and gravity has been a long standing area of research starting by the work of Kawai, Lewellen and Tye (KLT) [59], to the recent discovery of Bern, Carrasco and Johansson (BCJ) [60, 61]. The BCJ-relations state that there exists a representation of the Yang-Mills amplitude (with or without supersymmetry) in terms of cubic graphs,

$$\mathcal{A}_{YM} = \sum_{i \in \text{cubic}} \frac{n_i c_i}{s_i} \quad (4.2)$$

where n_i are kinematic numerators, c_i are color factors and s_i is the denominator of the cubic graph given by Feynman propagators BCJ [60, 61] states that whenever the color factors c_i satisfy the Jacobi identity $c_i + c_j = c_k$ then the numerators satisfy the same relation $n_i + n_j = n_k$. Once we have (4.2) the gravity amplitude can be then obtained by the simple formula¹,

$$\mathcal{M}_{GR} = \sum_{i \in \text{cubic}} \frac{n_i \tilde{n}_i}{s_i} \quad (4.3)$$

where the set of numerators \tilde{n}_i do not necessarily have to satisfy the Jacobi relation, i.e. they can belong to a non-BCJ representation of the Yang-Mills amplitude. If we start with two copies of $\mathcal{N} = 4$ sYM then we obtain an $\mathcal{N} = 8$ SUGRA amplitude. There is a dictionary for the squaring relations between amplitudes in lower supersymmetric theories with different matter content (see e.g. [62]) and even for some effective field theories [63]. The BCJ-relations are a conjecture which was proven for tree-level amplitudes and tested up to high loop order for loop amplitudes, there it is a statement about integrands.

In order to prove that the amplitudes in $\mathcal{N} = 8$ SUGRA have only logarithmic singularities (except poles at infinity) we first assume the loop BCJ-relations (4.3) and also the statement that the $\mathcal{N} = 4$ sYM amplitudes can always be expressed in (4.1) where all basis integrals \mathcal{I}_k have only logarithmic singularities. This is certainly true up to high loop order [49–51] and it is reasonable to assume it holds to all loops. Then we can use one copy of the Yang-Mills amplitude written in this manifest $d \log$ form, and the other copy written in the BCJ-form (4.2). The gravity amplitude is then given by (4.3). While the numerator in the $d \log$ form \tilde{n}_i already guarantees that term-by-term all singularities are logarithmic in the Yang-Mills amplitude, then the expression (4.3) will also have only logarithmic singularities term-by-term. This

¹There is a natural identification of coupling constants which does not play a role in our discussion and we suppress them altogether.

is not true for poles at infinity as adding the extra numerator n_i introduces further loop momentum dependence in the numerator, but for finite ℓ all singularities stay logarithmic. This argument was already used in [50] but we repeat it here because it is in perfect agreement with the results we get from the gravity on-shell diagrams.

Let us comment on the poles at infinity explicitly. The on-shell diagrams have higher poles at infinite momentum and this is what we also expect from the BCJ-form (4.3) as adding two copies of n_i increases the power counting in the numerator. Indeed, looking at the explicit results we can see that the loop amplitudes in $\mathcal{N} = 8$ SUGRA do have poles at infinity. The simplest example is the 3-loop four-point amplitude. The cut represented by the following (non-reduced) on-shell diagram,

$$\text{Diagram 1} \xrightarrow{a \rightarrow 0} \text{Diagram 2} \sim \int \frac{dz}{z} \times F(\text{X}), \quad (4.4)$$

has a pole at $z \rightarrow \infty$, corresponding to $\ell \rightarrow \infty$. The detailed expression for the z -independent function $F(\text{X})$ is not particularly illuminating but can be obtained by either gluing together tree-amplitudes or by evaluating the known representation of the gravity amplitude [64] on the cut. Starting with the cut on the left hand side of (4.4), the relevant loop momentum ℓ is parameterized by two degrees of freedom, a and z ,

$$\ell(a, z) = (1 - a)\lambda_1\tilde{\lambda}_1 + a\lambda_2\tilde{\lambda}_2 + \frac{a(1 - a)}{z}\lambda_2\tilde{\lambda}_1 + z\lambda_1\tilde{\lambda}_2.$$

By localizing $a \rightarrow 0$, we go to the maximal cut and select a unique contribution where no further cancellations are possible. Since we are on the maximal cut, the gravity numerator in the diagrammatic expansion of the amplitude can be obtained by squaring the respective $\mathcal{N} = 4$ sYM numerator of any representation and we take [50],

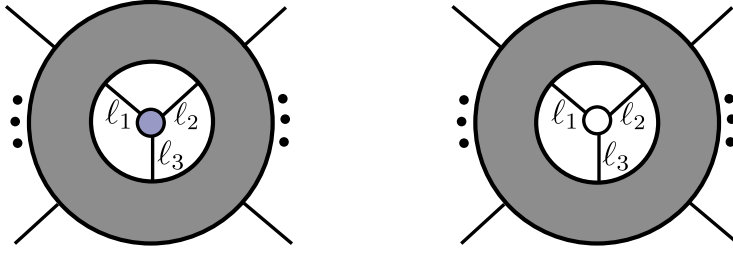
$$N^{\text{GR}} \Big|_{\text{cut}} \sim stu\mathcal{M}_4^{\text{tree}} \cdot \left[s(\ell + p_4)^2 \right]_{\text{cut}}^2,$$

where $stu\mathcal{M}_4^{\text{tree}} = \left(\frac{[34][41]}{\langle 12 \rangle \langle 23 \rangle} \right)^2$ is the totally crossing symmetric prefactor depending on external kinematics only. The important observation is that the integrand in (4.4) behaves like $\frac{dz}{z}$ leading to the pole at infinity in $\ell(z) \rightarrow \infty$. At higher loops we even get multiple poles at infinity [50]. In general, poles at infinity can indicate potential UV-divergencies after integration as is the case for the bubble integral. However, a

direct association of poles at infinity with a UV-divergence is not possible. The triangle integral for example also has a pole at infinity but it is UV-finite. Finding a precise rule between the interplay of poles at infinity and the UV-behavior of gravity amplitudes is an active area of research and would have a direct bearing on the UV-finiteness question of $\mathcal{N} = 8$ SUGRA [65].

4.3 Collinear behavior

Based on the numerator factors in the Grassmannian formula for gravity on-shell diagrams (2.20) it is natural to conjecture that the residue of loop amplitudes on cuts that involve a three-point vertex (where the grey blob is any tree or loop amplitude),



factorize in a particular way,

$$\mathcal{M} = \langle \ell_1 \ell_2 \rangle \cdot \mathcal{R} \quad \text{for MHV vertex, i.e. } \widetilde{\lambda}_{\ell_1} \sim \widetilde{\lambda}_{\ell_2} \sim \widetilde{\lambda}_{\ell_3}, \quad (4.5)$$

$$\mathcal{M} = [\ell_1 \ell_2] \cdot \overline{\mathcal{R}} \quad \text{for } \overline{\text{MHV}} \text{ vertex, i.e. } \lambda_{\ell_1} \sim \lambda_{\ell_2} \sim \lambda_{\ell_3}, \quad (4.6)$$

where \mathcal{R} and $\overline{\mathcal{R}}$ are functions regular in $\langle \ell_1 \ell_2 \rangle$ and $[\ell_1 \ell_2]$ respectively. If both ℓ_1 and ℓ_2 are external particles this reduces to the well known behavior of gravity amplitudes in the collinear limit [66, 67],

$$\mathcal{M} \sim \frac{[12]}{\langle 12 \rangle} \cdot \widetilde{\mathcal{M}} \quad \text{for } \langle 12 \rangle \rightarrow 0, \quad \mathcal{M} \sim \frac{\langle 12 \rangle}{[12]} \cdot \widetilde{\mathcal{M}} \quad \text{for } [12] \rightarrow 0. \quad (4.7)$$

Let us stress that our claim is more general as one or both of the ℓ_k can be loop momenta and there is no such statement available in the literature. It is fair to say that this statement does not follow from formula (2.20) for on-shell diagrams but it is rather motivated by it. The reason is that the lower cuts can not be directly written as the sums of on-shell diagrams. There are some extra $1/s_{ij}$ factors one has to add when going from on-shell diagram to generalized cuts, and therefore our statement does not immediately apply to the other cuts. If we calculate the residue of the amplitude on the cut when the three point amplitude (say MHV) factorizes then this piece factorizes $\langle \ell_1 \ell_2 \rangle$ but it is not guaranteed that the rest of the diagram does not give additional $\frac{1}{\langle \ell_1 \ell_2 \rangle}$ and cancel this factor. This does not happen in the case of on-shell diagrams but

it could for generalized cuts. Our conjecture is that indeed it does not happen and any cut of the amplitude of this type would be proportional to $\langle \ell_1 \ell_2 \rangle$. We will test this conjecture explicitly on several examples.

Four point one-loop

The four-point one-loop $\mathcal{N} = 8$ SUGRA amplitude was first given by Green, Schwarz and Brink [68] as a sum of three box integrals²,

$$\mathcal{M}_4^1(1234) = i stu \mathcal{M}_4^{\text{tree}}(1234) \left[I_4^1(s, t) + I_4^1(t, u) + I_4^1(u, s) \right], \quad (4.8)$$

where the corresponding tree amplitude $\mathcal{M}_4^{\text{tree}}(1234)$ carries the helicity information. Multiplying by stu one finds the totally permutation invariant four-point gravity prefactor, see e.g. [69],

$$stu \mathcal{M}_4^{\text{tree}}(1234) = \underbrace{\left(\frac{[34][41]}{\langle 12 \rangle \langle 23 \rangle} \right)^2}_{\equiv \mathcal{K}_8}. \quad (4.9)$$

The one-loop box integrals $I_4^1(-, -)$ are defined without the usual st -type normalization which was put into the permutation invariant prefactor \mathcal{K}_8 . All integrals have numerator $N = 1$ and therefore do not have unit leading singularity $\pm 1, 0$ on all residues,

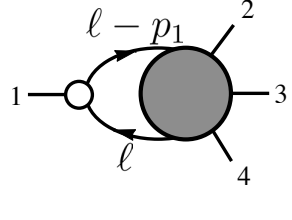
$$I_4^1(s; t) = \text{Box}(s, t), \quad I_4^1(t; u) = \text{Box}(t, u), \quad I_4^1(u; s) = \text{Box}(u, s) \quad (4.10)$$

As there is no unique origin in loop momentum space, there is a general problem how to label the loop momentum ℓ in individual diagrams; we will come back to this point shortly. In the definition (4.10), we chose an arbitrary origin for the loop momentum routing in each of the three boxes.

Let us consider a double cut of the amplitude where $\ell^2 = (\ell - p_1)^2 = 0$ which chooses natural labels on the cut. For complex momenta, there are two solutions to the on-shell conditions. Here we choose the one with $\ell = \lambda_1 \tilde{\lambda}_\ell$ for some $\tilde{\lambda}_\ell$, which

²The gravitational coupling constant $(\kappa/2)^{n-2}$ for n -pt tree level amplitudes and $(\kappa/2)^n$ for n -pt one-loop amplitudes will be suppressed ($\kappa = \sqrt{32\pi G_N}$).

corresponds to the cut diagram. The grey blob corresponds to five point $(L - 1)$ loop amplitude, but in our case $L = 1$ and it is just tree,



$$(4.11)$$

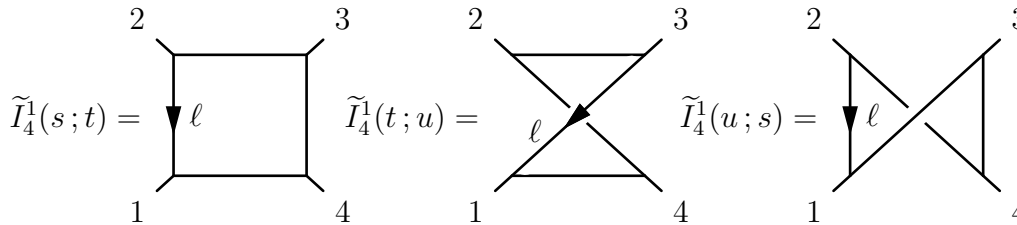
Note that for $\ell^2 = 0$ the loop momentum ℓ becomes null and can be written as, $\ell = \lambda_{\ell} \tilde{\lambda}_{\ell}$ so that the other propagator factorizes, $(\ell - p_1)^2 = \langle \ell 1 \rangle [\ell 1]$. The solution we chose sets $\langle \ell 1 \rangle = 0$ and the Jacobian of this double cut is,

$$\mathcal{J} = \frac{1}{[\ell 1]}. \quad (4.12)$$

Using the box-expansion of the one-loop amplitude (4.8) we can calculate the residue on this cut for all three boxes (4.10) individually and get,

$$\begin{aligned} & \left[I_4^1(s, t) + I_4^1(t, u) + I_4^1(u, s) \right] \Big|_{\ell = \lambda_1 \tilde{\lambda}_{\ell}} = \\ &= \frac{1}{[\ell 1]} \left[\frac{1}{(\ell - p_1 - p_2)^2 (\ell + p_4)^2} + \frac{1}{(\ell - p_1 - p_3)^2 (\ell + p_4)^2} + \frac{1}{(\ell - p_1 - p_2)^2 (\ell + p_3)^2} \right] \Big|_{\ell = \lambda_1 \tilde{\lambda}_{\ell}} \\ &= \frac{1}{[\ell 1]} \left[\frac{1}{\langle 12 \rangle ([12] - [\ell 2]) \langle 14 \rangle [\ell 4]} + \frac{1}{\langle 13 \rangle ([13] - [\ell 3]) \langle 14 \rangle [\ell 4]} + \frac{1}{\langle 12 \rangle ([12] - [\ell 2]) \langle 13 \rangle [\ell 3]} \right] \\ &= \frac{[\ell 1] \cdot [34] \langle 14 \rangle}{[\ell 1] \cdot [\ell 3] [\ell 4] ([12] - [\ell 2]) ([13] - [\ell 3]) \langle 12 \rangle \langle 13 \rangle \langle 14 \rangle} \end{aligned} \quad (4.13)$$

From the Jacobian (4.12), each term contains a factor $\frac{1}{[\ell 1]}$ but combining all three boxes we generate an expression with $[\ell 1]$ in the numerator which cancels \mathcal{J} . However, this is not enough. Our conjecture was that on this cut the amplitude behaves like $\sim [\ell 1]$. The computation above seems to immediately contradict the conjecture but due to labeling issues mentioned earlier, the calculation is incomplete. In labeling the box diagrams in (4.10), we made a particular choice. We could have labeled the three boxes in a different way,



$$(4.14)$$

which gives a different residue on the cut (4.11),

$$\begin{aligned}
& \left[\tilde{I}_4^1(s, t) + \tilde{I}_4^1(t, u) + \tilde{I}_4^1(u, s) \right] \Big|_{\ell=\lambda_1 \tilde{\lambda}_\ell} = \\
& \frac{1}{[\ell 1]} \left[\frac{1}{(\ell - p_1 - p_4)^2 (\ell + p_2)^2} + \frac{1}{(\ell - p_1 - p_4)^2 (\ell + p_3)^2} + \frac{1}{(\ell - p_1 - p_3)^2 (\ell + p_2)^2} \right] \Big|_{\ell=\lambda_1 \tilde{\lambda}_\ell} \\
& = \frac{[\ell 1] \cdot [23] \langle 12 \rangle}{[\ell 1] \cdot [\ell 2] [\ell 3] ([13] - [\ell 3]) ([14] - [\ell 4]) \langle 12 \rangle \langle 13 \rangle \langle 14 \rangle} \quad (4.15)
\end{aligned}$$

Summing over both expression (4.13) and (4.15) (we should include a factor $\frac{1}{2}$ but that is irrelevant here) and using $[23] \langle 12 \rangle = [34] \langle 14 \rangle$ we get

$$\mathcal{M}_4^1(1234) \Big|_{\ell=\lambda_1 \tilde{\lambda}_\ell} \sim \frac{[23] \langle 12 \rangle [24] \cdot [\ell 1]^2}{[\ell 1] \cdot [\ell 2] [\ell 3] [\ell 4] ([12] - [\ell 2]) ([13] - [\ell 3]) ([14] - [\ell 4]) \langle 12 \rangle \langle 13 \rangle \langle 14 \rangle}, \quad (4.16)$$

so that our conjecture indeed passes this check as the amplitude vanishes for $[\ell 1] = 0$, i.e. $\ell \sim p_1$. This example clearly demonstrates that the symmetrization over labels is important in getting the correct result. Note that the sum over six terms naturally arises when one starts directly from the cut-picture (4.11). To get all contributions, one is instructed to expand the five-point tree in all possible ways and find the contributions of all basis integrals. This procedure automatically takes into account all labellings of loop-momenta.

Four point two-loop

We will now test the same property for the four-point two-loop amplitude which is given as a sum of planar- and non-planar double-box integrals including a numerator factor [70],

$$\begin{aligned}
I_{(1234)}^{(P)} &= s^2 \times \text{[Planar Double-Box Diagram]} \\
I_{(1234)}^{(NP)} &= s^2 \times \text{[Non-Planar Double-Box Diagram]} \quad (4.17)
\end{aligned}$$

$$\mathcal{M}_4^2 = \frac{\mathcal{K}_8}{4} \sum_{\sigma \in \mathfrak{S}_4} \left[I_\sigma^{(P)} + I_\sigma^{(NP)} \right], \quad (4.18)$$

where the sum over σ runs over all 24 permutations of \mathfrak{S}_4 .

The full calculation can be performed numerically, but here we present a simplified version in which we calculate the residue on $\ell^2 = \langle \ell 1 \rangle = [\ell 1] = 0$ which sets $\ell = \alpha p_1$ directly. When combining all pieces, the numerator again generates $[\ell 1]^2$ so that the residue on the $\frac{1}{[\ell 1]}$ pole vanishes quadratically. Going directly to the kinematic region where $\ell = \alpha p_1$ we are only able to see a pure vanishing $\mathcal{M}_4^2(1234)\big|_{\ell=\alpha p_1} = 0$, but even this weaker statement requires an intricate cancellation between a large number of different terms.

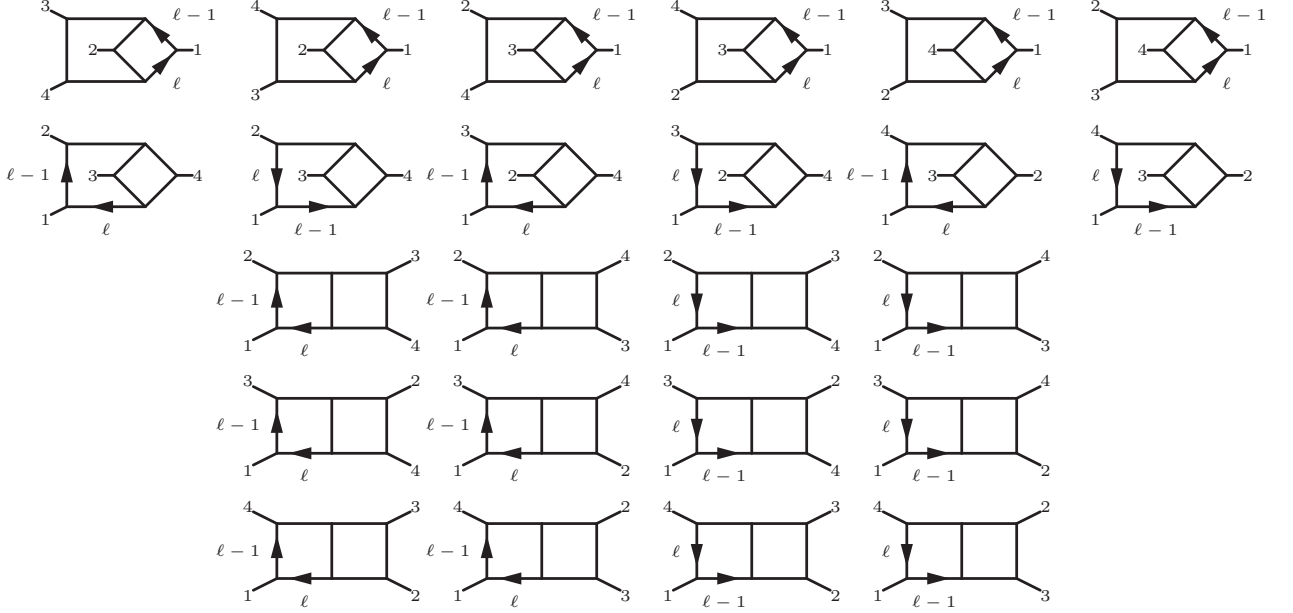


Figure 1. Contributing integrals on the collinear cut.

Starting with the collinear cut $\ell^2 = \langle \ell 1 \rangle = [\ell 1] = 0$, there are 24 terms contributing. If we look at the nonplanar integrals, for collinear kinematics $\ell = \alpha p_1$, we can use one factor of s of the numerator (4.17) to decompose the pentagon as a sum of boxes. This

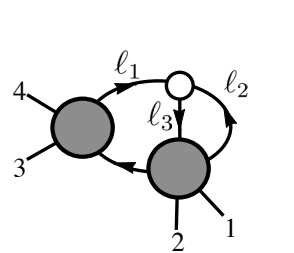
is only possible for this special kinematics.

$$\begin{aligned}
& \begin{array}{c} \alpha 1 \quad 2 \quad (1-\alpha)1 \\ \diagdown \quad \diagup \\ s \\ \diagup \quad \diagdown \\ 4 \quad 3 \end{array} = \frac{1}{\alpha} \times \begin{array}{c} 2 \quad (1-\alpha)1 \\ \diagdown \quad \diagup \\ \alpha 1+4 \quad 3 \end{array} - \frac{1}{\alpha} \times \begin{array}{c} \alpha 1+2 \quad (1-\alpha)1 \\ \diagdown \quad \diagup \\ 4 \quad 3 \end{array} \\
& - \frac{1}{1-\alpha} \times \begin{array}{c} \alpha 1 \quad (1-\alpha)1+2 \\ \diagdown \quad \diagup \\ 4 \quad 3 \end{array} + \frac{1}{1-\alpha} \times \begin{array}{c} \alpha 1 \quad 2 \\ \diagdown \quad \diagup \\ 4 \quad (1-\alpha)1+3 \end{array}
\end{aligned} \tag{4.19}$$

If one uses the pentagon decomposition (4.19) on all nonplanar integrals in the first line of Fig. 1 and rewrites the $\frac{1}{\alpha}$ and $\frac{1}{1-\alpha}$ coefficients of the boxes in terms of propagators by multiplying and dividing by appropriate Mandelstam variables, one can see that all the planar double-boxes cancel. Each nonplanar integral in the first line cancels exactly two planar double boxes, so that the counting works perfectly. The remaining two terms of the decomposition that come with a plus sign are almost as straight-forward. One has to collect all these terms and re-express them as non-planar integrals. Combined with the non-planar integrals of the second line in Fig. 1, one can show that they always come in the combination $(s+t+u) = 0$ so that they also cancel. This concludes our calculation and indeed we find our conjecture to hold. All signs work out such that the two-loop four-point amplitude in fact vanishes on the collinear cut $\ell = \alpha p_1$.

Internal collinear region

Finally we can show one more example when the collinear region is between internal loops only corresponding to the cases described in the beginning of Sec. 4.3. The simplest example where we can study this kinematic region is for the two-loop four-point amplitude discussed above. Instead of going to the triple cut $\ell_1^2 = \ell_2^2 = (\ell_1 + \ell_2)^2 = 0$ we can cut one more propagator to simplify the analysis by limiting the number of contributing terms,



$$\tag{4.20}$$

Parameterizing the cut solution on $\ell_1^2 = \ell_2^2 = 0$ as

$$\ell_1 = \left[\lambda_1 + \alpha_1 \lambda_2 \right] \left[\alpha_2 \tilde{\lambda}_2 + \alpha_3 \tilde{\lambda}_1 \right], \quad \ell_2 = \left[\lambda_1 + \beta_1 \lambda_2 \right] \left[\beta_2 \tilde{\lambda}_2 + \beta_3 \tilde{\lambda}_1 \right],$$

the third propagator $\ell_3^2 \equiv (\ell_1 + \ell_2)^2$ factorizes and we cut $\langle \ell_1 \ell_2 \rangle = 0$ by setting $\beta_1 = \alpha_1$. The remaining part of the factorized propagator becomes, $[\ell_1 \ell_2] = [21](\alpha_2 \beta_3 - \alpha_3 \beta_2)$. As mentioned before, we simplify our life by further cutting $(\ell_1 + p_3 + p_4)^2 = 0$ which sets $\alpha_3 = 1 - \alpha_1 \alpha_2$.

Blowing up the blobs in (4.20) into planar and non-planar double-boxes (4.17) of different labels and combining all $(8 + 4)$ terms, we checked numerically that the two-loop amplitude behaves as,

$$M_4^2 \Big|_{\langle \ell_1 \ell_2 \rangle = 0} \sim \frac{[\ell_1 \ell_2]^2}{[\ell_1 \ell_2]} \cdot \overline{\mathcal{R}}, \quad (4.21)$$

where the numerator generates the $[\ell_1 \ell_2]^2$ -factor consistent with our conjecture.

5 Conclusion

In this paper we studied on-shell diagrams in gravity theories. We wrote a Grassmannian representation using edge variables and our formulation includes a non-trivial numerator factor in the measure as well as higher degree poles in the denominator. We showed that all higher poles correspond to cases where internal momenta in the loop are sent to infinity while all erasable edges are represented by single poles only. The numerator factor can be interpreted as a set of collinearity conditions on the on-shell momenta. We provide several examples in the paper for both leading singularities as well as diagrams with unfixed parameters. Because on-shell diagrams are also cuts of gravity loop amplitudes it is natural to conjecture that loop amplitudes share the same properties. We tested this conjecture on the cases of 1-loop and 2-loop amplitudes in $\mathcal{N} = 8$ SUGRA and found a perfect agreement. Unlike in the Yang-Mills case these properties of on-shell diagrams can not be implemented term-by-term and require non-trivial cancellations between diagrams (even at four-point one-loop).

There was one aspect of gravity on-shell diagrams we did not discuss in more detail: *poles at infinity*. While absent in gauge theory they are present in gravity on-shell diagrams as poles of arbitrary degree. Poles at finite locations in momentum space correspond to erasing edges in on-shell diagrams but there is no such interpretation for poles at infinity. It is not clear how to embed them in the Grassmannian and what is the on-shell diagrammatic interpretation for them. This also prevents us from writing homological identities between different on-shell diagrams which was an important

ingredient in the Yang-Mills case. Finally, the poles at infinity are closely related to the UV-behavior of gravity loop amplitudes and further study of their role in on-shell diagrams could lead to new insights there.

Note: While this work was completed, [71] appeared which has some overlap with our results.

Acknowledgments

We thank Nima Arkani-Hamed, Zvi Bern, Jacob Bourjaily, Sean Litsey and James Stankowicz for interesting discussions. Most figures are drawn with the Mathematica package [72]. E. H. is supported in part by a Dominic Orr Graduate Fellowship and by DOE Grant # DE-SC0011632.

References

- [1] R. Britto, F. Cachazo, and B. Feng, *New recursion relations for tree amplitudes of gluons*, *Nucl.Phys.* **B715** (2005) 499–522, [[hep-th/0412308](#)].
- [2] R. Britto, F. Cachazo, B. Feng, and E. Witten, *Direct proof of tree-level recursion relation in Yang-Mills theory*, *Phys.Rev.Lett.* **94** (2005) 181602, [[hep-th/0501052](#)].
- [3] Z. Bern, L. J. Dixon, D. C. Dunbar, and D. A. Kosower, *One loop n point gauge theory amplitudes, unitarity and collinear limits*, *Nucl.Phys.* **B425** (1994) 217–260, [[hep-ph/9403226](#)].
- [4] Z. Bern, L. J. Dixon, D. C. Dunbar, and D. A. Kosower, *Fusing gauge theory tree amplitudes into loop amplitudes*, *Nucl.Phys.* **B435** (1995) 59–101, [[hep-ph/9409265](#)].
- [5] Z. Bern, J. Carrasco, H. Johansson, and D. Kosower, *Maximally supersymmetric planar Yang-Mills amplitudes at five loops*, *Phys.Rev.* **D76** (2007) 125020, [[arXiv:0705.1864](#)].
- [6] R. Britto, F. Cachazo, and B. Feng, *Generalized unitarity and one-loop amplitudes in $N=4$ super-Yang-Mills*, *Nucl.Phys.* **B725** (2005) 275–305, [[hep-th/0412103](#)].
- [7] F. Cachazo, *Sharpening The Leading Singularity*, [[arXiv:0803.1988](#)].
- [8] N. Arkani-Hamed, J. L. Bourjaily, F. Cachazo, S. Caron-Huot, and J. Trnka, *The All-Loop Integrand For Scattering Amplitudes in Planar $N=4$ SYM*, *JHEP* **1101** (2011) 041, [[arXiv:1008.2958](#)].
- [9] S. Caron-Huot, *Loops and trees*, *JHEP* **05** (2011) 080, [[arXiv:1007.3224](#)].
- [10] R. E. Cutkosky, *Singularities and discontinuities of Feynman amplitudes*, *J. Math. Phys.* **1** (1960) 429–433.
- [11] S. Mandelstam, *Determination of the pion - nucleon scattering amplitude from dispersion relations and unitarity. General theory*, *Phys. Rev.* **112** (1958) 1344–1360.

- [12] N. Arkani-Hamed, J. L. Bourjaily, F. Cachazo, A. B. Goncharov, A. Postnikov, and J. Trnka, *Scattering Amplitudes and the Positive Grassmannian*, [arXiv:1212.5605](#).
- [13] P. Benincasa and F. Cachazo, *Consistency Conditions on the S-Matrix of Massless Particles*, [arXiv:0705.4305](#).
- [14] E. Witten, *Perturbative gauge theory as a string theory in twistor space*, *Commun.Math.Phys.* **252** (2004) 189–258, [[hep-th/0312171](#)].
- [15] Z. Xu, D.-H. Zhang, and L. Chang, *Helicity Amplitudes for Multiple Bremsstrahlung in Massless Nonabelian Gauge Theories*, *Nucl. Phys.* **B291** (1987) 392.
- [16] J. Broedel and L. J. Dixon, *Color-kinematics duality and double-copy construction for amplitudes from higher-dimension operators*, *JHEP* **10** (2012) 091, [[arXiv:1208.0876](#)].
- [17] J. Drummond, J. Henn, G. Korchemsky, and E. Sokatchev, *Dual superconformal symmetry of scattering amplitudes in $N=4$ super-Yang-Mills theory*, *Nucl.Phys.* **B828** (2010) 317–374, [[arXiv:0807.1095](#)].
- [18] V. P. Nair, *A Current Algebra for Some Gauge Theory Amplitudes*, *Phys. Lett.* **B214** (1988) 215.
- [19] H. Elvang and Y.-t. Huang, *Scattering Amplitudes*, [arXiv:1308.1697](#).
- [20] A. P. Hodges, *Twistor diagrams for all tree amplitudes in gauge theory: A Helicity-independent formalism*, [hep-th/0512336](#).
- [21] A. Hodges, *Eliminating spurious poles from gauge-theoretic amplitudes*, *JHEP* **1305** (2013) 135, [[arXiv:0905.1473](#)].
- [22] A. Postnikov, *Total positivity, Grassmannians, and networks*, *ArXiv Mathematics e-prints* (Sept., 2006) [[math/0609764](#)].
- [23] N. Arkani-Hamed, F. Cachazo, C. Cheung, and J. Kaplan, *A Duality For The S Matrix*, *JHEP* **1003** (2010) 020, [[arXiv:0907.5418](#)].
- [24] N. Arkani-Hamed, F. Cachazo, and C. Cheung, *The Grassmannian Origin Of Dual Superconformal Invariance*, *JHEP* **1003** (2010) 036, [[arXiv:0909.0483](#)].
- [25] L. Mason and D. Skinner, *Dual Superconformal Invariance, Momentum Twistors and Grassmannians*, *JHEP* **0911** (2009) 045, [[arXiv:0909.0250](#)].
- [26] G. Lusztig, *Total positivity in partial flag manifolds*, *Represent. Theory* **2** (1998) 70–78.
- [27] A. Postnikov, D. Speyer, and L. Williams, *Matching polytopes, toric geometry, and the non-negative part of the Grassmannian*, *ArXiv e-prints* (June, 2007) [[arXiv:0706.2501](#)].
- [28] L. K. Williams, *Enumeration of totally positive Grassmann cells*, *ArXiv Mathematics e-prints* (July, 2003) [[math/0307271](#)].

- [29] A. B. Goncharov and R. Kenyon, *Dimers and cluster integrable systems*, *ArXiv e-prints* (July, 2011) [[arXiv:1107.5588](#)].
- [30] A. Knutson, T. Lam, and D. Speyer, *Positroid Varieties: Juggling and Geometry*, *ArXiv e-prints* (Nov., 2011) [[arXiv:1111.3660](#)].
- [31] J. M. Drummond, J. M. Henn, and J. Plefka, *Yangian symmetry of scattering amplitudes in $N=4$ super Yang-Mills theory*, *JHEP* **0905** (2009) 046, [[arXiv:0902.2987](#)].
- [32] J. Drummond, G. Korchemsky, and E. Sokatchev, *Conformal properties of four-gluon planar amplitudes and Wilson loops*, *Nucl.Phys.* **B795** (2008) 385–408, [[arXiv:0707.0243](#)].
- [33] L. Ferro, T. Lukowski, C. Meneghelli, J. Plefka, and M. Staudacher, *Harmonic R-matrices for Scattering Amplitudes and Spectral Regularization*, *Phys.Rev.Lett.* **110** (2013), no. 12 121602, [[arXiv:1212.0850](#)].
- [34] L. Ferro, T. Lukowski, C. Meneghelli, J. Plefka, and M. Staudacher, *Spectral Parameters for Scattering Amplitudes in $N=4$ Super Yang-Mills Theory*, *JHEP* **1401** (2014) 094, [[arXiv:1308.3494](#)].
- [35] N. Beisert, J. Broedel, and M. Rosso, *On Yangian-invariant regularization of deformed on-shell diagrams in $\mathcal{N} = 4$ super-Yang-Mills theory*, *J.Phys.* **A47** (2014) 365402, [[arXiv:1401.7274](#)].
- [36] J. Broedel, M. de Leeuw, and M. Rosso, *Deformed one-loop amplitudes in $N = 4$ super-Yang-Mills theory*, [arXiv:1406.4024](#).
- [37] A. Kotikov and L. Lipatov, *On the highest transcendentality in $N=4$ SUSY*, *Nucl.Phys.* **B769** (2007) 217–255, [[hep-th/0611204](#)].
- [38] B. Eden and M. Staudacher, *Integrability and transcendentality*, *J.Stat.Mech.* **0611** (2006) P11014, [[hep-th/0603157](#)].
- [39] N. Beisert, B. Eden, and M. Staudacher, *Transcendentality and Crossing*, *J.Stat.Mech.* **0701** (2007) P01021, [[hep-th/0610251](#)].
- [40] A. B. Goncharov, M. Spradlin, C. Vergu, and A. Volovich, *Classical Polylogarithms for Amplitudes and Wilson Loops*, *Phys.Rev.Lett.* **105** (2010) 151605, [[arXiv:1006.5703](#)].
- [41] J. Golden, A. B. Goncharov, M. Spradlin, C. Vergu, and A. Volovich, *Motivic Amplitudes and Cluster Coordinates*, *JHEP* **1401** (2014) 091, [[arXiv:1305.1617](#)].
- [42] J. M. Drummond, G. Papathanasiou, and M. Spradlin, *A Symbol of Uniqueness: The Cluster Bootstrap for the 3-Loop MHV Heptagon*, *JHEP* **03** (2015) 072, [[arXiv:1412.3763](#)].
- [43] D. Parker, A. Scherlis, M. Spradlin, and A. Volovich, *Hedgehog bases for A_n cluster*

- polylogarithms and an application to six-point amplitudes*, *JHEP* **11** (2015) 136, [[arXiv:1507.0195](#)].
- [44] L. J. Dixon, J. M. Drummond, M. von Hippel, and J. Pennington, *Hexagon functions and the three-loop remainder function*, *JHEP* **12** (2013) 049, [[arXiv:1308.2276](#)].
 - [45] L. J. Dixon and M. von Hippel, *Bootstrapping an NMHV amplitude through three loops*, *JHEP* **10** (2014) 065, [[arXiv:1408.1505](#)].
 - [46] L. J. Dixon, M. von Hippel, and A. J. McLeod, *The four-loop six-gluon NMHV ratio function*, [[arXiv:1509.0812](#)].
 - [47] N. Arkani-Hamed, J. L. Bourjaily, F. Cachazo, A. Postnikov, and J. Trnka, *On-Shell Structures of MHV Amplitudes Beyond the Planar Limit*, *JHEP* **06** (2015) 179, [[arXiv:1412.8475](#)].
 - [48] S. Franco, D. Galloni, B. Penante, and C. Wen, *Non-Planar On-Shell Diagrams*, *JHEP* **06** (2015) 199, [[arXiv:1502.0203](#)].
 - [49] N. Arkani-Hamed, J. L. Bourjaily, F. Cachazo, and J. Trnka, *Singularity Structure of Maximally Supersymmetric Scattering Amplitudes*, [[arXiv:1410.0354](#)].
 - [50] Z. Bern, E. Herrmann, S. Litsey, J. Stankowicz, and J. Trnka, *Logarithmic Singularities and Maximally Supersymmetric Amplitudes*, *JHEP* **06** (2015) 202, [[arXiv:1412.8584](#)].
 - [51] Z. Bern, E. Herrmann, S. Litsey, J. Stankowicz, and J. Trnka, *Evidence for a Nonplanar Amplituhedron*, [[arXiv:1512.0859](#)].
 - [52] S. Weinberg, *Photons and Gravitons in s Matrix Theory: Derivation of Charge Conservation and Equality of Gravitational and Inertial Mass*, *Phys. Rev.* **135** (1964) B1049–B1056.
 - [53] S. Weinberg, *Photons and gravitons in perturbation theory: Derivation of Maxwell's and Einstein's equations*, *Phys. Rev.* **138** (1965) B988–B1002.
 - [54] P. Benincasa, *On-shell diagrammatics and the perturbative structure of planar gauge theories*, [[arXiv:1510.0364](#)].
 - [55] J. Drummond, J. Henn, V. Smirnov, and E. Sokatchev, *Magic identities for conformal four-point integrals*, *JHEP* **0701** (2007) 064, [[hep-th/0607160](#)].
 - [56] L. F. Alday and J. M. Maldacena, *Gluon scattering amplitudes at strong coupling*, *JHEP* **0706** (2007) 064, [[arXiv:0705.0303](#)].
 - [57] N. Arkani-Hamed and J. Trnka, *The Amplituhedron*, *JHEP* **10** (2014) 030, [[arXiv:1312.2007](#)].
 - [58] N. Arkani-Hamed, A. Hodges, and J. Trnka, *Positive Amplitudes In The Amplituhedron*, *JHEP* **08** (2015) 030, [[arXiv:1412.8478](#)].

- [59] H. Kawai, D. Lewellen, and S. Tye, *A Relation Between Tree Amplitudes of Closed and Open Strings*, *Nucl.Phys.* **B269** (1986) 1.
- [60] Z. Bern, J. Carrasco, and H. Johansson, *New Relations for Gauge-Theory Amplitudes*, *Phys.Rev.* **D78** (2008) 085011, [[arXiv:0805.3993](#)].
- [61] Z. Bern, J. J. M. Carrasco, and H. Johansson, *Perturbative Quantum Gravity as a Double Copy of Gauge Theory*, *Phys.Rev.Lett.* **105** (2010) 061602, [[arXiv:1004.0476](#)].
- [62] H. Johansson and A. Ochirov, *Color-Kinematics Duality for QCD Amplitudes*, *JHEP* **01** (2016) 170, [[arXiv:1507.0033](#)].
- [63] G. Chen and Y.-J. Du, *Amplitude Relations in Non-linear Sigma Model*, *JHEP* **01** (2014) 061, [[arXiv:1311.1133](#)].
- [64] Z. Bern, J. Carrasco, L. J. Dixon, H. Johansson, and R. Roiban, *Manifest Ultraviolet Behavior for the Three-Loop Four-Point Amplitude of $N=8$ Supergravity*, *Phys.Rev.* **D78** (2008) 105019, [[arXiv:0808.4112](#)].
- [65] Z. Bern, L. J. Dixon, and R. Roiban, *Is $N = 8$ supergravity ultraviolet finite?*, *Phys. Lett.* **B644** (2007) 265–271, [[hep-th/0611086](#)].
- [66] Z. Bern, L. J. Dixon, M. Perelstein, and J. S. Rozowsky, *One loop n point helicity amplitudes in (selfdual) gravity*, *Phys. Lett.* **B444** (1998) 273–283, [[hep-th/9809160](#)].
- [67] Z. Bern, L. J. Dixon, M. Perelstein, and J. S. Rozowsky, *Multileg one loop gravity amplitudes from gauge theory*, *Nucl. Phys.* **B546** (1999) 423–479, [[hep-th/9811140](#)].
- [68] M. B. Green, J. H. Schwarz, and L. Brink, *$N=4$ Yang-Mills and $N=8$ Supergravity as Limits of String Theories*, *Nucl. Phys.* **B198** (1982) 474–492.
- [69] N. E. J. Bjerrum-Bohr, D. C. Dunbar, and H. Ita, *Six-point one-loop $N=8$ supergravity NMHV amplitudes and their IR-behaviour*, *Phys. Lett.* **B621** (2005) 183–194, [[hep-th/0503102](#)].
- [70] Z. Bern, L. J. Dixon, D. C. Dunbar, M. Perelstein, and J. S. Rozowsky, *On the relationship between Yang-Mills theory and gravity and its implication for ultraviolet divergences*, *Nucl. Phys.* **B530** (1998) 401–456, [[hep-th/9802162](#)].
- [71] P. Heslop and A. E. Lipstein, *On-Shell Diagrams for $N = 8$ Supergravity Amplitudes*, [[arXiv:1604.0304](#)].
- [72] J. L. Bourjaily, *Positroids, Plabic Graphs, and Scattering Amplitudes in Mathematica*, [[arXiv:1212.6974](#)].